Geomorphology 126 (2011) 279–296

Contents lists available at ScienceDirect

Geomorphology

journal homepage: www.elsevier.com/locate/geomorph

Modeling of hydroecological feedbacks predicts distinct classes of landscape pattern, process, and restoration potential in shallow aquatic ecosystems

Laurel G. Larsen *, Judson W. Harvey

National Research Program, U.S. Geological Survey, 430 National Center, Reston, VA 20192, United States

ARTICLE INFO

Article history:
Received 12 May 2009
Received in revised form 4 November 2009
Accepted 12 March 2010
Available online 21 March 2010

Keywords:
Wetlands
Patterned landscape
Modeling
Sediment transport
Feedback
Everglades

ABSTRACT

It is widely recognized that interactions between vegetation and flow cause the emergence of channel patterns that are distinct from the standard Schumm classification of river channels. Although landscape pattern is known to be linked to ecosystem services such as habitat provision, pollutant removal, and sustaining biodiversity, the mechanisms responsible for the development and stability of different landscape patterns in shallow, vegetated flows have remained poorly understood. Fortunately, recent advances have made possible large-scale models of flow through vegetated environments that can be run over a range of environmental variables and over timescales of millennia. We describe a new, quasi-3D cellular automata model that couples simulations of shallow-water flow, bed shear stresses, sediment transport, and vegetation dynamics in an efficient manner. That efficiency allowed us to apply the model widely in order to determine how different hydroecological feedbacks control landscape pattern and process in various types of wetlands and floodplains. Distinct classes of landscape pattern were uniquely associated with specific types of allogenic and autogenic drivers in wetland flows. Regular, anisotropically patterned wetlands were dominated by allogenic processes (i.e., processes driven by periodic high water levels and flow velocities that redistribute sediment), relative to autogenic processes (e.g., vegetation production, peat accretion, and gravitational erosion). These anistropically patterned wetlands are therefore particularly prone to hydrologic disturbance. Other classes of wetlands that emerged from simulated interactions included maze-patterned, amorphous, and topographically noisy marshes, open marsh with islands, banded string-pool sequences perpendicular to flow, parallel deep and narrow channels flanked by marsh, and ridge-and-slough patterned marsh oriented parallel to flow. Because vegetation both affects and responds to the balance between the transport capacity of the flow and sediment supply, these vegetated systems exhibit a feedback that is not dominant in most rivers. Consequently, unlike in most rivers, it is not possible to predict the "channel pattern" of a vegetated landscape based only on discharge characteristics and sediment supply; the antecedent vegetation pattern and vegetation dynamics must also be known.

In general, the stability of different wetland pattern types is most strongly related to factors controlling the erosion and deposition of sediment at vegetation patch edges, the magnitude of sediment redistribution by flow, patch elevation relative to water level, and the variability of erosion rates in vegetation patches with low flow-resistance. As we exemplify in our case-study of the Everglades ridge and slough landscape, feedback between flow and vegetation also causes hysteresis in landscape evolution trajectories that will affect the potential for landscape restoration. Namely, even if the hydrologic conditions that historically produced higher flows are restored, degraded portions of the ridge and slough landscape are unlikely to revert to their former patterning. As wetlands and floodplains worldwide become increasingly threatened by climate change and urbanization, the greater mechanistic understanding of landscape pattern and process that our analysis provides will improve our ability to forecast and manage the behavior of these ecosystems.

Published by Elsevier B.V.

1. Introduction

Navigable waterways serve a critical function in the world economy, providing savings of more than $7 billion annually in the United States alone over alternate means of shipping (ASCE, 2008). River channel classification arose in part out of the need to understand the mechanisms that maintain the long-term stability of these waterways (Garcia, 2007). By linking form and process, channel pattern classification and associated stability diagrams (Schumm, 1985) have led to an improved understanding of how channel slope, bankfull discharge, grain size, unit stream power, channel Froude numbers, and depth:width ratios interact to produce braided, meandering, straight, and anastamosed river channels.

* Corresponding author. Tel.: +1 703 648 5891; fax: +1 703 648 5484.
E-mail address: lglarsen@usgs.gov (L.G. Larsen).

0169-555X/$ – see front matter. Published by Elsevier B.V.
doi:10.1016/j.geomorph.2010.03.015

More recently, society has begun to place value on ecosystem services provided by wetlands and vegetated floodplains, including water storage and purification, habitat provision, climate regulation through carbon sequestration, and buffering of the coastal zone against storm surges and sea-level rise (Millennium Ecosystem Assessment, 2005). As with rivers, the value of wetland ecosystem services depends on landscape morphology. For example, wastewater treatment wetlands are most effective when vegetation is distributed homogeneously, to prevent the formation of short-circuiting channels (Lightbody et al., 2008). In contrast, heterogeneity in vegetation and topography is thought to be optimal for fish and other wildlife (Sartoris et al., 1999; Bays and Knight, 2002). Marsh grasses, benthic microalgae, and phytoplankton remove CO_2 from marsh ecosystems (Chmura et al., 2003; Bridgham et al., 2006), and the optimal configuration of these components for carbon sequestration in a flowing system is an ongoing research topic (Chmura et al., 2003).

Given current interest in wetland evaluation, restoration, and construction, an understanding of the drivers that create, maintain, and/or destroy wetland landscape patterns would have many applications. It is widely recognized that interactions between vegetation and flowing water produce landscape patterns distinct from the standard Schumm (1985) classification of river channel pattern. For instance, vegetation can inhibit the development of braided streams by enhancing bank resistance to erosion (Millar, 2000; Murray and Paola, 2003; Tal and Paola, 2007) and can cause development of an anabranching channel pattern, characterized by parallel channels that are stable over long timescales (Murray and Paola, 2003; Tal et al., 2004; Huang and Nanson, 2007). In some boreal bogs, feedback among vegetation, soil, flow, nutrients, and/or soil hydraulic properties can cause development of striped string-pool patterning oriented perpendicular to the flow (Swanson and Grigal, 1988; Couwenberg and Joosten, 2005; Eppinga et al., 2009b). Other regularly patterned wetlands, like the ridge and slough landscape of the Florida Everglades, develop with an orientation parallel to the flow direction, a feature thought to arise from feedbacks involving flow, sediment redistribution, vegetation dynamics, and peat accretion (Larsen et al., 2007). Tidal channels that develop on nascent tidal flats also exhibit a parallel, multiple-thread morphology due to feedback among flow, sediment transport, and vegetative resistance to flow (Temmerman et al., 2007). Brinson (1993) devised a classification system for these and other wetland landscape patterns. What is lacking in the published literature is a mechanistic understanding of conditions under which the different landscape/channel pattern types in vegetated flows are stable and how hydroecological feedbacks promote pattern development.

Studies of interactions between riparian vegetation and river channels are widespread (Mertes et al., 1995; Hupp and Osterkamp, 1996; Istanbulluoglu and Bras, 2005), and some have resulted in refined stability diagrams that account for vegetation in predicting channel pattern for alluvial rivers (Millar, 2000; Tal et al., 2004). Evaluating the stability of different landscape/channel pattern types in wetlands is more complex; while flow, sediment transport, and lithology are the chief drivers of river geomorphology, nutrient availability and uptake by vegetation (Rietkerk et al., 2004b; Eppinga et al., 2008), autogenic organic sediment accumulation (Nungesser, 2003; Larsen et al., 2007; Eppinga et al., 2008), and subsurface flow (Swanson and Grigal, 1988; Couwenberg and Joosten, 2005) can also govern pattern formation in wetlands. Because of generally slow flow and regular surface-water inundation of vegetation, lotic wetlands tend to exhibit a stronger bi-directional feedback between vegetation and flow (Leonard and Luther, 1995; Leonard and Reed, 2002; Nepf, 2004) that can further diversify landscape/channel pattern.

This paper presents a quasi-3D cellular automata model designed to improve our understanding of how feedback among flow, sediment transport, vegetation dynamics, and autogenic organic sediment accumulation causes different wetland landscape patterns to form and become stable. It performs coupled simulations of flow velocities, sediment transport, vegetation dynamics, and autogenic peat accretion. Several key feedbacks arise from the interactions among these drivers (Larsen et al., 2007). Under a sediment-flow-vegetation feedback, the deposition of sediment decreases local water levels, which suppresses sediment erosion and improves conditions for the growth of vegetation that further resists flow. The resulting increase in vegetative drag promotes additional sediment deposition in a positive-feedback response. Under a differential peat accretion feedback, peat accumulates most rapidly in dense, high-flow-resistance vegetation communities at intermediate water depths. In deeper conditions, vegetation growth becomes limited, and little organic matter is deposited. In shallower conditions, aeration of the substrate leads to oxidation of organic matter that limits peat accumulation. Since local peat elevations are inversely proportional to local water depths, these interactions serve as a negative feedback that cause the elevation of the high-flow-resistance vegetation community to converge to an equilibrium relative to the mean water level.

The cellular automata modeling approach we used to simulate these complex hydroecological feedbacks afforded computational savings that enabled thorough exploration of the stability of different landscape/channel patterns over wide ranges in several parameters. These input parameters (Table 1) included abiotic drivers such as water-surface slope, water depth, duration/frequency of pulsed flow events, sediment entrainment threshold, and sediment dispersivity, and biological drivers such as rates of vegetation propagation, the equilibrium elevation of vegetation communities, and rates of organic matter production and decomposition. Even without including different particle size distributions or densities or more than two vegetation communities, the model predicted almost the full range of landscape pattern types and landforms found in wetlands across the world (i.e., Fig. 1). Finally, using the Florida Everglades as a case-study, we evaluated the possibility for multiple stable states, which describes the condition in which two or more different landscape/channel patterns can be stable under environmental conditions that are identical except for the antecedent vegetation distribution (Beisner et al., 2003). An understanding of this phenomenon is important in predicting how wetland ecosystems will respond to climate change and urbanization, as well as the potential success of restoration efforts (Rietkerk et al., 2004a; Suding et al., 2004; Eppinga et al., 2009a).

2. Regional setting

Wetlands where autogenic organic sediment production and allogenic sediment transport govern landscape evolution are common at most latitudes throughout the world. Examples include tidal marshes, fens, coastal or inland river deltas such as the Okavango, inland swamps, and floodplain wetlands such as the Pantanal and the Everglades. Our model tests a broad range of environmental parameters (Table 1), making our work applicable to many of these low-gradient wetlands. However, the model also simulated interactions among vegetation communities, velocity profiles, and resulting bed shear stress using computational relationships developed specifically for two vegetation communities in the Everglades (Harvey et al., 2009; Larsen et al., 2009c). Because development of these relationships had considerable time, data collection, and validation requirements, we assumed that Everglades ridge and slough vegetation communities interacted with flow in a manner similar to densely and sparsely vegetated patches elsewhere. In this way, our findings are generalizable to a global range of wetlands while having particular applicability to the Everglades.

Centered at 26° 0″ N and 80° 45″ W, the 500,000 ha Everglades is one of the world's few low-latitude peatlands, with soil that is approximately 90% organic in the central part of the system (Gleason

Table 1
RASCAL model inputs and ranges.

Input parameter	Symbol in this paper	Values or range of values	Supporting source
Annual duration of high-flow events		0–21 days	
Initial surface-water level	$Z_{s,\mathrm{orig}}$	40–90 cm	Willard and Cronin, 2007
Water surface slope	S	3.0×10^{-5}–1.0×10^{-4}	National Research Council, 2003
Bed sediment diffusion coefficient (for erosion by gravity)	D_{sed}	High-resistance community: 2–300 $\mathrm{cm^2\ yr^{-1}}$ Low-resistance community: 20–4000 $\mathrm{cm^2\ yr^{-1}}$	Larsen et al., 2007
Initial relative high-resistance vegetation community coverage	A	0.005–0.250	
Critical shear stress for entrainment of bed sediment	τ_e	0.01, 0.02 Pa	Larsen et al., 2009a
Scaling factor affecting maximum peat accretion rate of high-resistance community	S_1	0.1–23	Larsen et al., 2007
Scaling factor affecting equilibrium elevation of high-resistance community	S_2	0.6–1.5	National Research Council, 2003; Larsen et al., 2007
Scaling factor for lateral vegetative propagation and below-ground biomass expansion	f	0.05–0.30	
Scaling factor for maximum y-direction velocity	$\max(\overline{u}_y)$	$\mathrm{mean}(\overline{u}_x)$, $0.5[\mathrm{mean}(\overline{u}_x)+\max(\overline{u}_x)]$	
Effective suspended sediment settling velocity	w_s	0.11 $\mathrm{cm\ s^{-1}}$	Larsen et al., 2009b
Sediment entrainment coefficient	M	When using $\tau_e=0.01$ Pa: 2.2×10^{-8} $\mathrm{g\,cm^{-2}\,s^{-1}}$. Otherwise: 1.3×10^{-7} $\mathrm{g\,cm^{-2}\,s^{-1}}$	Larsen et al., 2009a
Sediment entrainment exponent	n	When using $\tau_e=0.01$ Pa: 1.6. Otherwise: 1.3	Larsen et al., 2009a
Soil bulk density	ρ_b	0.06 $\mathrm{g\ cm^{-3}}$	Harvey et al., 2004
Mean annual evapotranspiration in low-resistance vegetation community	E_l	134.9 $\mathrm{cm\ yr^{-1}}$	German, 2000
Mean annual evapotranspiration in high-resistance vegetation community	E_h	118.4 $\mathrm{cm\ yr^{-1}}$	German, 2000
Soil porosity	θ	0.90	Myers, 1999

and Stone, 1994). As in other low-latitude peatlands, generally high water tables prohibit the complete oxidation of organic material, allowing peat buildup. Approximately two-thirds of the historical extent of the Everglades exhibited an undulating ridge and slough topography aligned parallel to flow (National Research Council, 2003). Ridges, up to 20 cm higher than sloughs in the present system, are colonized dominantly by dense emergent *Cladium jamaicense* (sawgrass). Sloughs have more diverse and generally lower-density vegetation that includes emergent *Eleocharis* (spikerush) and floating *Utricularia* spp. (bladderwort) that is usually associated with periphyton. Because of its larger frontal area, ridge vegetation has a higher resistance to flow than slough vegetation. Presently sloughs transport approximately 86% of the flow in the Everglades (Harvey et al., 2009). In this sense, the ridge and slough landscape is analogous to high-resistance tidal marshes with intervening low-resistance channels (French and Stoddart, 1992; Christiansen et al., 2000; Temmerman et al., 2007), high-resistance *Sphagnum* strings on striped fens with intervening low-resistance pools (Swanson and Grigal, 1988; Couwenberg and Joosten, 2005), and high-resistance tree islands interspersed among lower-resistance marsh grass in many floodplain wetland complexes (Wetzel, 2002; Bazante et al., 2006). Tree islands are also found within the Everglades ridge and slough landscape but are thought to arise from different feedbacks (Wetzel et al., 2005; Givnish et al., 2008) and are not a prime focus of this paper.

Everglades water tables fluctuate seasonally, from around 75 cm above the slough surface during the wet summer months (May–October), to within a few cm of the slough surface during the dry winter months (November–April) (Fennema et al., 1994). Despite high water tables, flows in the present system are slow, with laminar to transitional stem Reynolds numbers (Saiers et al., 2003) and slough velocities that average 0.4 $\mathrm{cm\ s^{-1}}$, with a maximum value of 5 $\mathrm{cm\ s^{-1}}$ measured during a hurricane (Harvey et al., 2009). These slow flows arise from a combination of the high vegetative flow resistance (Lee et al., 2004; Harvey and McCormick, 2009), the low bed slope (approximately 3–6×10^{-5}), and even lower water-surface slopes, which are as low as 1×10^{-5} in the central Everglades (Harvey et al., 2009). Relative to bed slopes, water-surface slopes are low because of impoundment. Levees and canals were constructed throughout the twentieth century to drain and compartmentalize portions of the Everglades for agriculture, provide flood control, and support water resources development. As a result, present flows are 2.5 to 4 times smaller than historically (Marshall et al., 2009).

Because of anthropogenic reductions in flow velocities and water levels, the ridge and slough landscape has undergone a catastrophic shift in landscape pattern structure, from a highly heterogeneous, flow-parallel structure to a more homogeneous structure, characterized by *C. jamaicense* monocultures and low topographic variability (National Research Council, 2003). Since the heterogeneity and well-connected sloughs of the historic ridge and slough landscape are valued for habitat provision, fish migration, and sustenance of wading bird colonies (Ogden, 2005), restoration of the ridge and slough pattern structure is a goal of the $10.9 billion Comprehensive Everglades Restoration Plan. However, there remains a fundamental lack of understanding of how hydroecological feedbacks historically maintained stable, heterogeneous patterning for millennia (Bernhardt and Willard, 2009) and now contribute to the ongoing evolution of this landscape.

3. Methods: model development

The large spatial and long temporal scales of landscape evolution make it difficult to understand controls on landscape evolution from field observations only. As an alternative, scaled physical models (e.g., Doeschl-Wilson and Ashmore, 2005; Tal and Paola, 2007) or numerical models (e.g., Istanbulluoglu and Bras, 2005) are commonly used. Numerical modeling has the advantage of permitting thorough analysis of the effects of multiple combinations of input parameters with relatively little time investment. By turning certain rules or processes in numerical models on or off, the most parsimonious set of processes that are essential for the development of a particular landscape type can be evaluated (e.g., Murray and Paola, 2002).

Several researchers have developed process-based models of interactions among flow, vegetation, and sediment transport in tidal marshes (Temmerman et al., 2005; D'Alpaos et al., 2007; Kirwan and Murray, 2007). However, these models have not been extended to simulations of other wetland types, in part because they do not explicitly simulate the effects of vegetation communities on flow or bed shear stress. To fully incorporate the feedback among flow, sediment transport, and vegetation, our model, RASCAL (*R*idge *a*nd

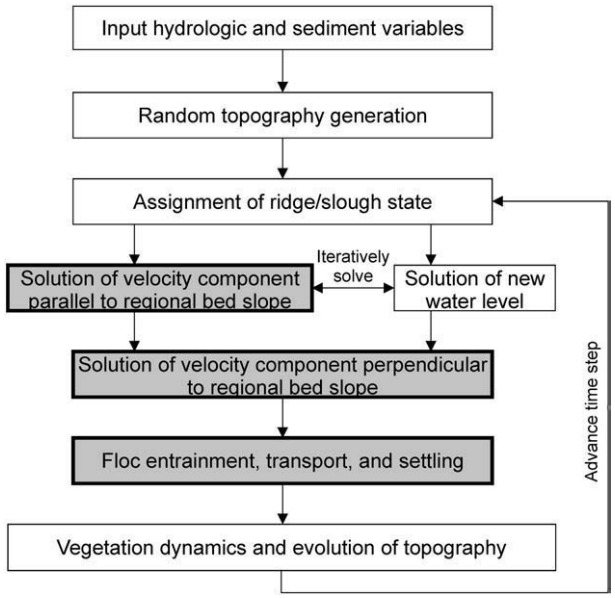

Fig. 2. Modularized structure of the RASCAL model. Different modules, which collectively simulate interactions among flow, sediment transport, and vegetation dynamics, operate over different timescales. Boxes depicted in gray operate only during pulses of high flow in which bed shear stresses are sufficient to entrain sediment. Other boxes operate continuously. A complete model time step is defined as the period of time over which the topography remains approximately static with respect to evolution of the flow field.

*S*lough *C*ellular *A*utomata *L*andscape, after the system for which it was originally developed) is the first coupled ecogeomorphological model that solves for a distribution of bed shear stresses that governs differential sediment erosion and deposition in high-flow-resistance and low-flow-resistance vegetation communities. Because this solution can be computationally expensive, we adopted a cellular automata-based modeling approach. Cellular automata are widely used in studies of landscape evolution (Fonstad, 2006), including studies of interactions among vegetation, geomorphology, and flow (Murray and Paola, 2003; Parsons and Fonstad, 2007). As a rule-based modeling scheme in which cells switch between two or more states (e.g., vegetation communities), cellular automata are computationally efficient yet can reproduce the complex feedbacks that cause landscape patterning (Wootton, 2001; Fonstad, 2006). Because of the simplifications of scale and process complexity involved in cellular automata modeling, these models are best used to compare relative outcomes and generate hypotheses for further quantitative testing in the field.

3.1. Model overview

RASCAL is modularized (Fig. 2), designed for easy and adaptable mix-and-match coupling between hydraulic, geomorphic, and ecological variables. It accepts a suite of user inputs (Table 1) that govern the initial topographic and vegetation distribution, a water-surface slope typical of high-flow periods, an initial water level, and various sediment physical properties and parameters governing rates of peat production. The model simulates a repeating 1.27 km × 1.86 km block of a larger landscape through the imposition of doubly periodic (i.e., wrapping) boundary conditions. The longer dimension (the *x*-dimension) is parallel to the bed slope. Discretized into cells of length 10 m parallel to the flow direction and width 5 m, the domain size was chosen to encompass three average modern ridges and sloughs in length and width.

Seasonality is incorporated into the model through high-flow pulses and intervening low-flow periods. During the annual high-flow pulse, which has a duration specified as an input parameter, bed shear stresses in sloughs are above the sediment entrainment threshold, and all modules are active. Bed shear stress is a dependent variable, calculated from the imposed high-flow discharge and water-surface slope. During low flows, sediment is not redistributed across the landscape, but topography can evolve through autogenic peat production processes, gravitational erosion of topographic gradients, and vegetative propagation/below-ground biomass expansion. These processes depend only on water level, so flow velocities are not simulated during this period. Although annual variability in flow is accounted for, interannual variability is assumed negligible. Specifically, the total annual discharge supplying high-flow events remains constant from year to year. The simulation maintains a water balance in which this constant supply of flow is partitioned among evapotranspiration, subsurface storage, and surface flow. Partitioning of water among these compartments changes as vegetation and topography evolve, causing the water level associated with high-flow events to stray from the initial condition as the simulation progresses.

Table 2
Summary statistics of vegetation communities examined.

Community	Mean *a* of emergent vegetation, cm^{-1}	Mean *d* of emergent vegetation, mm
High-resistance	6.7×10^{-3}	2.2
Low-resistance	1.9×10^{-2}	2.0
Perturbed low-resistance (with greater density of emergent vegetation)	2.8×10^{-2}	7.8

3.2. Assignment of cell state

RASCAL domain cells were assigned one of two states: a high-flow-resistance state typical of Everglades ridges and a low-flow-resistance state typical of Everglades sloughs. Profiles of vegetation frontal areas per unit volume (a) and stem diameters (d) for each cell state were averaged from representative clip-plots harvested across the Everglades (Larsen et al., 2009c, summarized in Table 2). Consistent with vegetation zonation in most marshes worldwide (FitzGerald et al., 2008), transitions between cell vegetation states in the model were governed predominantly by soil elevation relative to water level. Based on water depth surveys in Everglades ridge and slough vegetation communities (Givnish et al., 2008; Eppinga et al., 2009b), cells with a local depth of at most 46.2 cm were deterministically assigned the high-flow-resistance state (ridge), whereas those with a local depth of at least 65.4 cm were deterministically assigned the low-flow-resistance state (slough). Cells with intermediate local depth were stochastically assigned to the high- or low-resistance state with an error-function-shaped probability distribution curve, where the probability of being assigned to the high-resistance state was 50% greater if any of the eight neighboring cells or the next cell in

Fig. 1. Worldwide diversity of wetland landscape patterns and RASCAL simulation outcomes. Simulation outcomes (left image of each pair) were classified into general (lettered) and specific (numbered) groups (Table 4) using a hierarchical clustering analysis based on a variety of landscape indices calculated with FRAGSTATS (see Fig. 3). Outcomes are planform views of vegetation state, where white represents the high-flow-resistance, high-elevation vegetation community and black is the low-resistance vegetation community. Although many actual landscape morphologies (right image of each pair, obtained from Google Earth) closely resemble RASCAL simulation outcomes, these patterns are not unique to feedback among flows, vegetation dynamics, and sediment transport and can also arise from nutrient-governed or subsurface flow-governed feedbacks. At the upper right, the topography of the model domain at an advanced stage of model evolution, which shows the development of deep and narrow preferential channels, is depicted.

the upstream direction was high-resistance vegetation, or if the cell of interest was high-resistance vegetation in the previous time step. Overall, it was assumed that vegetation state changed rapidly relative to topographic changes.

3.3. Flow velocity solution

Rules for routing flow in the model are based on the depth-averaged conservation and momentum equations for flow through vegetation (Nepf, 2004). Vegetation is incorporated through a porosity term and through drag coefficients and longitudinal and transverse eddy viscosities based on vegetation architecture (unique to each vegetation community) and stem wake theory (Nepf, 1999; White and Nepf, 2003; Lightbody and Nepf, 2006a). We disregard the Reynolds stress term in the momentum equation, which is negligible in vegetation wake-dominated regions and is significant at vegetated/unvegetated interfaces only at depth-based Reynolds numbers on the order of 10^3–10^4 (White and Nepf, 2008), higher than the flows we consider here. As with other coupled models of flow and sediment transport through vegetation (Van De Wiel and Darby, 2004; Wu and Wang, 2004; D'Alpaos et al., 2007), we assume that the topography is static within each time step, and we solve for the steady-state flow field.

Boundary-value solutions of the steady-state conservation and momentum equation are computationally expensive (Parsons and Fonstad, 2007). RASCAL overcomes this obstacle by simplifying the equations into routing rules that result in an approximate and qualitatively robust flow field, based on assumptions that apply to low-gradient wetlands. One assumption is that of a planar water surface (i.e., uniform water-surface slope over the model domain), which allows local water depths (H) to be solved from soil elevations and reduces the dimensionality of the continuity and momentum equations by one. The second assumption is that flows parallel to the bed slope are primarily controlled by the balance between gravity and vegetative drag (Nepf, 2004; Neumeier and Ciavola, 2004; Harvey et al., 2009) and secondarily by longitudinal dispersion of momentum, particularly at interfaces (Lightbody and Nepf, 2006b). This assumption, as we will show, allows an approximate solution for the x-component of velocity ($\overline{u}_x$, where the overbar here and elsewhere denotes a depth-averaged quantity) independently of the y-component ($\overline{u}_y$).

Another key efficiency gain in RASCAL is its use of lookup tables for fluid dynamical quantities (Table 3) computed from a validated, one-dimensional, Reynolds-averaged Navier–Stokes (RANS) solution of high-resolution velocity profiles and bed shear stresses under steady, uniform conditions for separate ridge and slough vegetation communities (Larsen et al., 2009c). In complex vegetation canopies, Larsen (2008) showed that computation of these quantities from depth-averaged velocities are subject to large errors, necessitating the detailed solution. The lookup tables provide these quantities as discrete functions of some combination of the depth-averaged velocity magnitude ($\overline{u}$), depth-averaged velocity components (e.g., $\overline{u}_x$), and H. Use of these discrete functions assumes that for a given velocity and H, the values of these quantities under uniform flow are sufficiently similar to those for the same velocity and H in nonuniform flow (Larsen et al., 2009c).

The values of $\overline{u}_x$ and H are computed sequentially, with each subsequent estimate better approximating the solution. At the first step (subscript "0"), $\overline{u}_x$ is computed assuming vegetative drag is equal to gravitational forcing. Then, $\overline{u}_x$ is uniquely determined from the RANS lookup table for vegetative drag, using the input initial value of H for the first time step or the initial estimate of H for subsequent time steps (see *Transitioning to the Next Time Step*). Assuming that y-direction convection and bed drag are negligible compared to the other terms in the momentum balance, and that the x- and y-direction eddy viscosities can be approximated as the longitudinal and transverse eddy diffusivities, the error in the momentum equation is next computed as:

$$\varepsilon = \underbrace{-\overline{(1-ad)u_x}\frac{\partial \overline{u}_x}{\partial x}}_{x-\text{direction convection}} + \underbrace{g\overline{\left(1-\frac{\pi}{4}ad\right)}S}_{\text{gravitational forcing}} \underbrace{-\frac{1}{2}\overline{C_D a u_x^2}}_{\text{vegetative drag}} + \underbrace{\overline{(1-ad)}\frac{\partial}{\partial x}\left(D_l\frac{\partial \overline{u}_x}{\partial x}\right)}_{x-\text{direction dispersion}} + \underbrace{\overline{(1-ad)}\frac{\partial}{\partial y}\left(D_{tr}\frac{\partial \overline{u}_x}{\partial y}\right)}_{y-\text{direction dispersion,}} \quad (1)$$

where g is the acceleration due to gravity, S is the water-surface slope, and the other terms are defined in Table 3.

In the next step (subscript "1"), the error in the momentum equation is absorbed by the drag term so that

$$\frac{1}{2}\overline{(C_D a u_x^2)}_1 \approx \frac{1}{2}\overline{(C_D a u_x^2)}_0 + \varepsilon. \quad (2)$$

The solution for $\overline{u}_{x,1}$ at model domain row j and column k depends on the shape of the lookup table surface for $\overline{C_D a u_x^2}$, and for most vegetation communities can be approximated by (Larsen, 2008):

$$\overline{u}_{x,1,jk} = \left(\overline{u}_{x,0,jk}^{\sigma} + \frac{b_{jk}\varepsilon_{jk}}{\alpha_{jk}}\right)^{1/\sigma}, \quad (3)$$

where σ and α describe the shape of the lookup table surface and b is a damping factor for the cell that ranges between zero and one. The damping factor, which ensures a stable solution for $\overline{u}_{x,1}$, is most important during early time steps, when the topography is noisy and relatively large errors can result from the longitudinal diffusive transfer of momentum. It is chosen so that the gain or loss of velocity in the cell of interest is no more than half of the largest difference between the cell of interest and the neighboring cells in the upstream and downstream direction (Larsen, 2008).

With the $\overline{u}_{x,1}$ estimate, the $\overline{u}_x$ velocity field is considered sufficiently well-conditioned to calculate discharge. For each row j, the calculated row discharge per unit width (Q_{calc}) is $\sum_k \overline{u_{x,1,jk}(1-ad)}_{jk} H_{jk} k_{max}^{-1}$, where k is the column (i.e., constant y) index and k_{max} is the total number of columns in the model domain. At this point, the water surface level (and hence the matrix of H, equal to the water surface level minus the local surface elevation) is adjusted so that the mean Q_{calc} averaged across rows is equal to the imposed discharge per unit width for high-flow periods (Q). Q is originally solved as the mean Q_{calc} resulting from the initial values of H and S input to the model and is then adjusted at the end of each time step to maintain a water balance (see *Transitioning to the Next Time Step*).

The final estimate of x-direction velocity, $\overline{u}_{x,2}$, is computed to ensure that the value of Q_{calc} for each row equals Q, so that mass is conserved. Physically, the increase or decrease in velocity required to satisfy the constant discharge criterion would be absorbed primarily by cells in the vicinity of the vegetation patch transition that are experiencing substantial transfer of momentum in the y-direction through convection or diffusion. Consequently, flows are adjusted in proportion to $\overline{u}_{x,1,jk}|\overline{u}_{x,1,j,k-1} - \overline{u}_{x,1,j,k+1}|$. The resulting equation for $\overline{u}_{x,2}$ is:

$$\overline{u}_{x,2,jk} = \left(\overline{u}_{x,0,jk}^{\sigma} + \frac{b_{jk}\varepsilon_{jk} + \chi_j \overline{u}_{x,1,jk}|\overline{u}_{x,1,j,k-1} - \overline{u}_{x,1,j,k+1}|}{\alpha_{jk}}\right)^{1/\sigma}. \quad (4)$$

χ_j is the constant of proportionality for the change in velocity across the row, computed iteratively by finding the zero of $Q - \sum_k \overline{u_{x,2,jk}(1-ad)}_{jk} H_{jk} k_{max}^{-1}$ to machine precision.

Characteristic of cellular automata models of surface-water flow is that local processes in the neighborhood of each cell of interest govern

Table 3
Model Functions and RANS model inputs.

Quantity	Description	Equation	Source(s)	Notes
τ_0	Bed shear stress	$\rho g H S - \frac{1}{2}\rho H \overline{C_D a u^2}\left(\overline{1-\frac{\pi}{4}ad}\right)^{-1}$	Larsen et al., 2009c	RANS lookup table input, function of $\overline{u}$, H. ρ = density of water.
$\frac{1}{2}\overline{C_D a u_x^2}$	Vegetative drag force per unit area		Larsen et al., 2009c	RANS lookup table input, function of $\overline{u}_x$, H
C_D	Drag coefficient	$2K_0 Re^{-k}(ad)^{-0.5}$	Harvey et al., 2009	K_0 and k are empirical, vegetation community-specific constants. Re = stem-based Reynolds number
$\overline{1-ad}$	Vegetation porosity term, vertical plane		Nepf, 2004	RANS lookup table input, function of H
$\overline{1-\frac{\pi}{4}ad}$	Vegetation porosity term, horizontal plane		Nepf, 2004	RANS lookup table input, function of H
$\overline{u_x(1-ad)}$	Coefficient for convection term in momentum equation		Nepf, 2004	RANS lookup table input, function of $\overline{u}_x$, H
D_l	Longitudinal eddy diffusivity (assumed equal to longitudinal eddy viscosity)	$\overline{ud\sqrt{\frac{C_D^3 Re_t}{128}}\psi + \frac{C_D ad}{4(1-ad)} + \frac{\omega\kappa}{St}ad^2 u\varsigma - \frac{\overline{u}}{dH}\int_0^H\left(\frac{u}{\overline{u}}-1\right)\int_0^z\left(\frac{d\overline{u}}{k}\right)\int_0^z\left(\frac{u}{\overline{u}}-1\right)dzdzdz} + \nu$	White and Nepf, 2003; Nepf, 2004; Lightbody and Nepf, 2006a; Larsen, 2008	RANS lookup table input, function of $\overline{u}$, H. Re_t = turbulent stem Reynolds number. St = Strouhal number. $\psi = 1$ when $Re > 200$, otherwise 0. $\varsigma = 1$ when $Re > 47$, otherwise 0. ω and κ = constants from Duan and Wiggins (1997). ν = kinematic viscosity
K	Vertical eddy viscosity	$\frac{0.81}{4}(C_D a d^4)^{1/3}u$: wake region $0.41^2\ell^2\frac{\partial u}{\partial z}$: turbulent boundary layer ν: laminar boundary layer	Nepf et al., 1997; Nepf, 1999; Pope, 2000	See Larsen, 2008 for description of different regions. ℓ = von Karman-Prandtl length scale.
D_{tr}	Transverse eddy diffusivity (assumed equal to transverse eddy viscosity)	$0.81\overline{(C_D a d^4)^{1/3}u} + \nu + 0.5\overline{uad^2}$	Nepf et al., 1997; Nepf, 1999	RANS lookup table input, function of $\overline{u}$, H
D_x	x-direction eddy diffusivity	$\frac{\overline{u}_x}{\overline{u}}D_l + \frac{\overline{u}_y}{\overline{u}}D_{tr}$		
D_y	y-direction eddy diffusivity	$\frac{\overline{u}_y}{\overline{u}}D_l + \frac{\overline{u}_x}{\overline{u}}D_{tr}$		
$\overline{u}$	Magnitude of velocity vector	$\sqrt{\overline{u}_x^2 + \overline{u}_y^2}$		
c	Correction factor to relate depth-averaged concentration to concentration at reference location $\tilde{z}$	$\frac{H}{\exp\left(w_s\int_0^{\tilde{z}}K^{-1}dz\right)\int_0^H\exp\left(-w_s\int_0^z K^{-1}dz\right)dz}$	Larsen, 2008	
DPA	Differential peat accretion regression	$S_1\left[c_1\left(\frac{\eta_*}{S_2}\right)^3 + c_2\left(\frac{\eta_*}{S_2}\right)^2 + c_3\left(\frac{\eta_*}{S_2}\right) + c_4\right]$: high-productivity vegetation 0: low-productivity vegetation	Larsen et al., 2007	S_1 and S_2 = scaling factors for maximum rate of peat accretion and equilibrium elevation, respectively. c_1–c_4 = empirical coefficients defined in Larsen et al. 2007.
η^*	Soil elevation of high-resistance community, adjusted for changes in water level	$\eta - Z_s + Z_{s,\mathrm{orig}}$	Larsen, 2008	Z_s = elevation of water surface. $Z_{s,\mathrm{orig}}$ = initial water surface elevation

how flow is routed through that cell (Parsons and Fonstad, 2007). Likewise, in RASCAL the solution of the $\overline{u}_x$ flow field governs how water is transferred transversely through the cell in order to best approximate the continuity equation. This rule-based approach to approximating $\overline{u}_y$ is designed to reproduce the topographic steering effect of flow divergence at the heads of high-resistance patches and convergence at the tails. Namely, zones ("units") of surplus x-direction discharge are routed laterally across the cell (e.g., at the heads of high-resistance patches, where relatively fast-moving water from upstream encounters relatively slow-moving water) to zones of deficit x-direction discharge via y-direction advection (see Fig. S1). To first order, the cellular automata model assumes that the y-direction advection is proportional to the negative of the slope of the excess discharge across the row:

$$\overline{u}_y = -\varpi\frac{\partial}{\partial y}\left(\frac{\partial\overline{u_x(1-ad)}H}{\partial x}\right), \tag{5}$$

where $\overline{\omega}$ is a constant of proportionality with the dimension of [L] that is solved to scale the maximum value of $|\overline{u}_y|$ to the $\overline{u}_x$ field. Namely, $\varpi = \max|\overline{u}_y| / \max\left|\frac{\partial}{\partial y}\left(\frac{\partial\overline{u_x(1-ad)}H}{\partial x}\right)\right|$, where $\max|\overline{u}_y|$ is a user-selected input (see Table 1).

3.4. Sediment transport solution

Based on the solution of $\overline{u}_x$ and $\overline{u}_y$, suspended sediment concentrations were estimated directly from a two-dimensional, depth-averaged advection-dispersion equation. Bedload was assumed to be zero, and we used an entrainment function for cohesive sediment aggregates (Winterwerp and van Kesteren, 2004). The solution was steady-state, meaning that for the period of high flow, the spatial distribution of depth-averaged suspended sediment concentrations ($\overline{C}$) was invariant. A steady-state solution was

obtained from the long-term solution of the transient advection–dispersion equation using an explicit, forward-difference algorithm with a dynamic time step that satisfied the Courant criterion for stability. A value of $\overline{C}$ at which the settling flux in each cell was equal to the entrainment flux was used to initialize the model, formulated as:

$$\frac{\partial \overline{C}H}{\partial t} = \underbrace{-w_s \overline{C} Hc}_{\text{settling}} \underbrace{-\overline{u_x(1-ad)}H\frac{\partial \overline{C}}{\partial x} - \overline{u_y(1-ad)}H\frac{\partial \overline{C}}{\partial y}}_{\text{advection}} + \underbrace{\overline{\left(1-\frac{\pi}{4}ad\right)}M\max\left[\left(\frac{\tau_0-\tau_e}{\tau_e}\right)^n, 0\right]}_{\text{entrainment}} + \underbrace{\overline{(1-ad)}\frac{\partial}{\partial x}\left(D_x\frac{\partial \overline{C}H}{\partial x}\right) + \overline{(1-ad)}\frac{\partial}{\partial y}\left(D_y\frac{\partial \overline{C}H}{\partial y}\right)}_{\text{dispersion}}, \quad (6)$$

where w_s is settling velocity, τ_0 is local bed shear stress (positively related to flow velocity), τ_e is the critical entrainment bed shear stress at which sediment first erodes (a spatially invariant constant), M and n are empirical constants, and c is a correction factor that accounts for the fact that deposition occurs by particle settling from near-bed portions of the sediment concentration profile, where values of concentration are typically high compared to the mean $\overline{C}$. Under supply-limited conditions, M is adjusted locally in eroding cells, based on flow pulse duration and bed sediment availability for erosion (i.e., the thickness of the erodible bed sediment layer), so that the cell erodes no more than the sediment available during the time step. To obtain c (Table 3), approximate concentration profiles are solved by integrating a one-dimensional advection–dispersion equation in which dispersion balances settling. Then, c is computed as the ratio of the suspended sediment calculation at a reference location ($\tilde{z}$) 1 cm above the bed to $\overline{C}$.

3.5. Changes in bed elevation

In addition to flow-dependent mechanisms, the bed elevation (η) changed at each time step because of gravitational erosion, autogenic peat accretion, and vegetative propagation/below-ground biomass expansion:

$$\frac{\partial \eta}{\partial t} = \underbrace{\frac{w_s \overline{C} c}{\rho_b}\overline{\left(1-\frac{\pi}{4}ad\right)}^{-1}}_{\text{settling/deposition}} \underbrace{-\frac{M}{\rho_b}\max\left[\left(\frac{\tau_0-\tau_e}{\tau_e}\right)^n, 0\right]}_{\text{erosion by flow}} + \underbrace{D_{\text{sed}}\left(\frac{\partial^2 \eta}{\partial x^2} + \frac{\partial^2 \eta}{\partial y^2}\right)}_{\text{gravitational erosion}} + \underbrace{DPA}_{\substack{\text{autogenic}\\ \text{peat}\\ \text{accretion}}} + \underbrace{f \cdot DPA_{\text{edge}}}_{\substack{\text{vegetative}\\ \text{propagation}}}, \quad (7)$$

where ρ_b is bulk density of the soil, D_{sed} is the diffusivity of the bed sediment, DPA is the differential peat accretion regression function (see Table 3), and the last term is described below. As in other models (Pasternack et al., 2001; Larsen et al., 2007), erosion of topographic gradients by gravity was simulated as a diffusion equation. Differential peat accretion on the high-elevation (and high-flow-resistance) vegetation patches relative to the low-elevation vegetation patches was simulated using a regression equation that summarizes the net effect of organic matter production and decomposition as a function of local soil surface elevation relative to the water surface (Table 3). The equation was derived from the results of the process-based PeatAccrete model, which simulated net peat accretion as a function of phosphorus concentration and hydrology at a time step of 0.001 days (Larsen et al., 2007). The convex-upward (i.e., humped) regression equation exhibited two roots in the range of elevations of interest, representing stable and unstable equilibrium elevations at which rates of organic matter production and decomposition were in balance. Between the roots of the equation, net peat accretion on high-elevation vegetation patches reached a maximum value near the optimum depth for community-specific primary production, where decomposition rates (which typically decrease with depth (DeBusk and Reddy, 1998)) were relatively low.

Although the form of the net peat accretion regression equation for high-elevation vegetation patches was based on Everglades data (Larsen et al., 2007), two key parameters — scaling factors that controlled the stable equilibrium elevation for the vegetation community and maximum net peat accretion rate — were retained as adjustable parameters to broaden the model's applicability to other vegetation communities (Table 1). Because the shape of organic matter production and decomposition curves as a function of water level are qualitatively similar across different wetland ecosystems (Morris et al., 2002; Givnish et al., 2008), we believe that this treatment is generally realistic. However, in situations where the low-elevation, low-resistance vegetation community is moderately productive and where soil elevations within this community are highly variable, this treatment would need to be modified by incorporating a separate regression equation for net peat production in the low-resistance vegetation community.

Changes in soil elevation due to vegetation productivity can also affect portions of the soil surface adjacent to actively growing patches of vegetation, both through vegetative propagation that expands the patch and through below-ground biomass growth that forces soil outward as well as upward (Miao and Sklar, 1998). RASCAL accounts for these processes by augmenting the elevation of cells adjacent to or diagonal from the edges of productive, high-resistance patches of vegetation. Within low-resistance, low-productivity edge cells abutting high-productivity cells along the longest cell dimension, autogenic soil growth is assumed to occur at a rate that is some fraction (f, see Table 1) of the rate of net relative peat accretion in the adjacent high-resistance cells (DPA_{edge} in equation 7). This fraction is adjusted downward for neighboring cells along the short cell dimension or in the diagonal position by a factor inversely proportional to the mean distance of the low-productivity cell from the center of the high-productivity cell (Larsen, 2008).

3.6. Transitioning to the next time step

After the topography is adjusted according to model rules, the water surface level is adjusted by volumetric displacement to arrive at the initial estimate of H for the next time step. The value of Q to be employed at the next time step of the model is adjusted to maintain a water balance. Assuming that subsurface flow is negligible compared to surface-water flow (Krest and Harvey, 2003), expanding patches of high-productivity vegetation affect the water available for surface-water flow primarily by changing the total rate of evapotranspiration, but also by removing a very small amount of surface water for subsurface storage during the process of soil formation. Thus,

$$\frac{\partial Q}{\partial t} = \frac{\partial A}{\partial t}(E_l - E_h)dx - \frac{\sum_j \sum_k \frac{\partial \eta}{\partial t}\theta dx}{k_{\max}\partial t}, \quad (8)$$

where A is the fractional aerial coverage of the high-productivity vegetation, E_l is the evapotranspiration rate of the low-resistance vegetation, E_h is the mean evapotranspiration rate of the high-resistance vegetation, and θ is the soil porosity.

3.7. Model execution

Starting from a low-flow-resistance initial condition (i.e., little emergent ridge-like vegetation), we ran the model 125 times using

different input parameters selected over ranges that are reasonable for low-gradient wetlands (Table 1) in a space-filling Latin hypercube design that precludes multicollinearity in the independent variables (Iman et al., 1981). This low-flow-resistance condition is typical of wetlands originating from an open-water or relatively wet state (e.g., through the process of terrestrialization) and is consistent with paleoecological records of the Everglades ridge and slough landscape (Bernhardt and Willard, 2009). For this part of our analysis, the topography was initialized randomly in accordance with a normal probability distribution. The standard deviation of the normal probability distribution of bed elevations was an input parameter that yielded a variable initial coverage of the high-resistance vegetation community. Elevations were relative to the plane of the mean bed slope.

Landscape indices (Fig. 3) that describe the complexity, orientation, distribution, connectivity, and shape of the two different vegetation communities were computed with FRAGSTATS (McGarigal et al., 2002). These indices were used as inputs in a hierarchical clustering analysis using an average linkage criterion (JMP statistical software, SAS, Inc.). The goal of the clustering analysis was to identify categories of landscape pattern in which the degree of coherent structure formation, direction(s) of pattern anisotropy, pattern wavelength, and patch cohesiveness, shape, and connectedness were consistent among members. Landscape outcomes with very short pairing distances in multivariate space were identified as members of the same group. If the next cluster in the hierarchy joined with the first at a position low on the dendrogram, this group would be incorporated into the first. At moderate joining distances, the second group would be joined with the first at the secondary (more general) level of clustering, but not at the most specific level. Clustering dendrograms also identified outliers, which typically were distinctive outcomes with strongly biomodal features that were not adequately characterized by the landscape indices. In these cases, it was apparent which outliers should be grouped with the landscape classes identified through automated clustering versus which were true outliers, in a class of their own.

Subsequent discriminant analyses and stepwise multiple logistic regression analyses based on the classes identified by clustering revealed the variables and regions of the input parameter space that best differentiated between and predicted the landscape pattern. These analyses were performed using standardized values of the input driving variables. The discriminant analyses, designed to differentiate between different classes of heterogeneous pattern structure, excluded outcomes that remained dominantly low-resistance vegetation, as many of the landscape indices of interest were not applicable to these model outcomes. We first attempted to explain differences between classes of landscape outcomes using main effects of the drivers alone, and if that method was found to produce statistically insignificant separation, we included interaction terms in the analysis.

Then, because many wetland landscapes experience shifts in environmental drivers, once some of the landscapes achieved equilibrium, we subjected them to perturbations. The three types of perturbations, acting solely or in combination, were similar to those imposed on the Everglades through anthropogenic activities (Bernhardt and Willard, 2009): decreased mean water levels (by 20 cm), decreased water-surface slopes (from 6.5×10^{-5} to 2.5×10^{-5}), and an increase in the abundance of high-resistance emergent vegetation (spikerush) in the low-resistance sloughs (see Table 2). Last, to evaluate the reversibility of perturbation trajectories (and, equivalently, to evaluate model behavior under high-flow-resistance initial conditions), we returned the perturbed models to the original set of environmental conditions driving landscape evolution. Before this "restoration" attempt, each perturbed model was brought to a consistent 60% coverage of the high-resistance vegetation community. In the Everglades, 55% coverage of ridges roughly distinguishes between portions of the ridge and slough landscape that remain well-preserved and portions that are actively degrading to a more homogeneous high-flow-resistance state (C. McVoy and M. Nungesser, pers. comm., 2009).

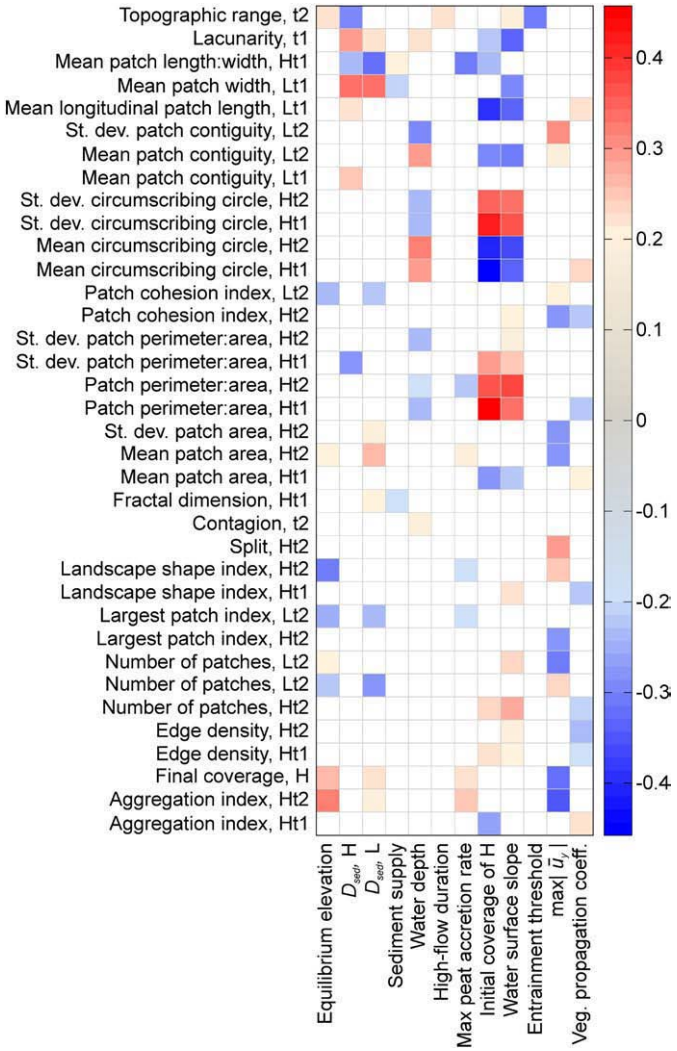

Fig. 3. Matrix of Spearman's correlations between input environmental drivers (*x*-axis) and output landscape indices. Red colors indicate a positive correlation between drivers and landscape indices; blue colors indicate a negative correlation. Only correlations that were significant at the $P<0.05$ level are depicted in color. In general, rows or columns that are highly colored suggest that the corresponding driver and/or response are sensitive or influential metrics, respectively. For a description of individual landscape indices, we refer readers to McGarigal et al. (2002). Landscape indices were acquired at two times of the landscape's development (*t*1 and *t*2), with *t*1 occurring at the point the landscape reached 28% coverage of the high-resistance patch and *t*2 occurring when the landscape reached 55% coverage (or the maximum for that particular outcome). The "*L*" or "*H*" tag preceding "*t*1" and "*t*2" indicates whether the metric was computed across the low-flow-resistance class or high-flow-resistance class. Contagion, lacunarity, and topographic range, in contrast, are computed across the landscape as a whole.

4. Results

4.1. Model assessment

Validation of bed shear stresses and the shape of velocity profiles used in the model was performed in a field flume experiment (Larsen 2008) and through comparison to published data (Lightbody and Nepf, 2006b). In both cases, predicted and observed bed shear stresses and normalized velocities were consistent within measurement error (Larsen 2008). Additionally, depth-averaged longitudinal flow

velocities measured in the best-preserved part of the present-day ridge and slough landscape (Harvey et al., 2009) fell along a 1:1 line with those predicted by RASCAL under identical conditions (Fig. 4). Slough velocities exhibited greater scatter along this line, likely because slough vegetation communities in the field are more highly variable in space and time (Harvey et al., 2009). We did not have measurements available to validate the $\overline{u}_y$ flow field, but the model rules produced a flow field that was physically realistic in a qualitative sense (Fig. 5), with flow divergence at high-resistance patch heads and convergence at the tails.

4.2. Diversity of model outcomes

Over millennia of evolution, simulated landscapes either remained nearly 100% low-resistance vegetation (7% of model runs), developed into a highly (<55% high-resistance vegetation) heterogeneous equilibrium combination of low-resistance vegetation patches interspersed among high-resistance vegetation patches (18% of model runs), or developed toward a nearly 100% high-resistance vegetation state (75% of model runs). Among the model runs that diverged toward the high-resistance state and those that remained heterogeneous, a wide-ranging variety of landscape structures emerged at intermediate stages of landscape evolution (Fig. 1). These structures differed most noticeably in their wavelength, orientation, topographic variance, and contiguity or connectedness.

Cluster analysis led to the identification of 13 general groups of landscape pattern (Table 4), which were further clustered into 28 distinctive groups. The most common type of landscape pattern during the evolution of the simulations (i.e., before divergence to a nearly-homogeneous high-resistance state occurred) was a combination of low-resistance and high-resistance vegetation states with little regularity in feature shape or occurrence, rounded edge zones, and an isotropic (i.e., non-directional) orientation. However, several of these landscapes did exhibit tendencies toward a more anisotropic configuration. Landscape outcomes in the general category of isotropic outcomes ("amorphous"), also differed in their degree of patch contiguity and wavelength; "maze-like" configurations had high contiguity of both patch types and often had a short wavelength (i.e., the mean length separating the nearest like patches) and low aggregation of low-resistance vegetation patches, whereas "island-like" configurations had low-contiguity patches of high-resistance vegetation interspersed among high-contiguity patches of low-resistance vegetation. The specific class of vegetation called "amorphous" exhibited features intermediate between the "maze-like" and "island-like" groups.

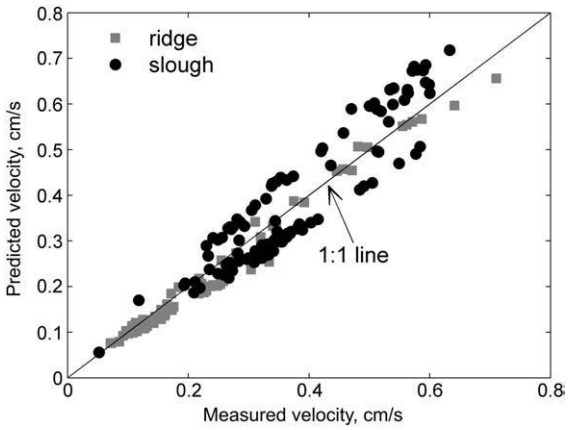

Fig. 4. Measured versus predicted mean longitudinal velocities in a relatively well-preserved part of the ridge and slough landscape. Daily average velocities were measured over two wet seasons with an acoustic Doppler velocimeter, as described in Harvey et al. (2009). Simultaneous measurements of water-surface slope and flow depths and one-time measurement of vegetation community architectures provided the inputs needed for this RASCAL model run.

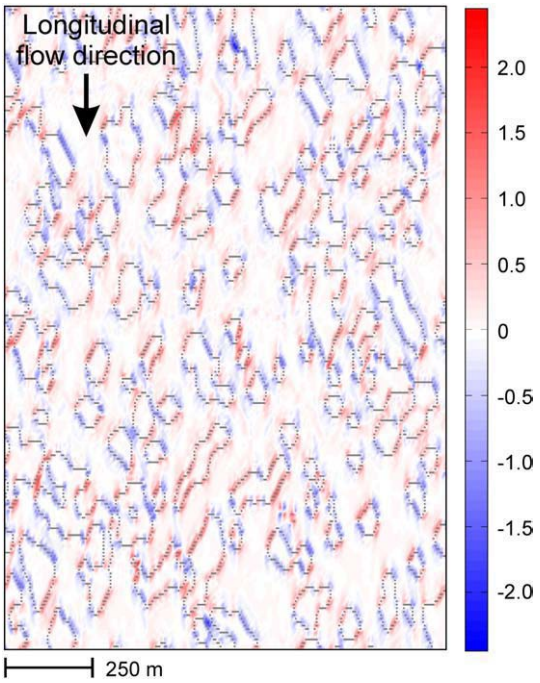

Fig. 5. Lateral component of flow velocity ($\overline{u}_y$, cm s^{-1}) in a heterogeneously vegetated landscape, showing convergence and divergence of flow around emerging patches of high-resistance vegetation (enclosed by dashed gray lines). The longitudinal flow direction, parallel to the regional bed slope, is from top to bottom. Positive lateral flow is to the left.

Other landscape types exhibited varying degrees of linear structure parallel or perpendicular to the flow direction, with a few landscapes exhibiting a bimodal mixture of high-resistance patches aligned parallel and perpendicular to the flow. Flow-parallel landscapes tended to contain ridges that were either approximately equal in width to sloughs or were substantially larger, while perpendicularly aligned landscapes contained high-resistance vegetation patches that were usually equal to or narrower than the low-resistance vegetation patches.

4.3. Controls on landscape evolution

4.3.1. Controls on patch stabilization

At early stages of landscape development, vegetation patches were not permanent, due to the stochastic colonization and die-off of high-resistance vegetation. Once patches reached a critical elevation (i.e., that at which high-resistance vegetation deterministically colonized the soil surface in the model), they were permanently stabilized, as the range of flows examined in our model were never sufficient to cause erosion within the high-resistance vegetation. However, this high-resistance patch stabilization and expansion never occurred in some of the models, which remained dominantly (>95%) or completely low-resistance vegetation.

Discriminant analysis poorly separated the landscapes that remained dominantly low-resistance vegetation from those that evolved high-resistance vegetation patches, even when interaction terms between different model inputs were included as variables in the analysis (Hotelling–Lawley test, $P=0.61$). However, a stepwise multiple logistic regression analysis, which is better able to detect variable sensitivity in a highly nonlinear response space, predicted the probability of patch development based on input variables and interactions at a significance of $P<0.0001$ and explained 63% of the variance in the dataset. The multiple logistic regression model

Table 4
Classification of wetland pattern structure predicted to arise from feedback among flow, sediment transport, and vegetation dynamics.

Specific class	Description	Number of model outcomes in category	General class
1	Short-wavelength flow-parallel patterning	3	A: Short-wavelength flow-parallel
2	Medium-wavelength flow-parallel patterning	2	
3	Short-wavelength with preferential parallel channels	2	
4	Short-wavelength dual-orientation	3	B: Dual-orientation
5	Long-wavelength dual-orientation	2	
6	Amorphous (low patch connectivity) with deep mixing zones	5	C: Amorphous
7	Medium-wavelength amorphous	2	
8	Circular islands with intervening vegetation strings	5	
9	Amorphous with flow-perpendicular tendency	3	
10	Amorphous with flow-parallel tendency	2	
11	Moderately elongated flow-parallel patches	2	D: Small elongated islands
12	Linear and circular islands	1	
13	Long-wavelength flow-parallel patches	1	E: Long-wavelength flow-parallel
14	Long-wavelength flow-perpendicular patches	3	F: Long-wavelength flow-perpendicular
15	Maze-like (highly connected patches) with somewhat perpendicular tendency	8	G: Maze-like
16	Maze-like with moderately perpendicular tendency	3	
17	Topographically noisy	3	
18	Maze-like with flow-parallel tendency	7	
19	Short-wavelength flow-perpendicular	2	H: Short-wavelength flow-perpendicular
20	Flow-parallel islands with perpendicular strings	2	
21	Flow-parallel ponds	2	I: Flow-parallel ponds
22	Incising parallel sloughs interspersed among convoluted ridges	3	J: Parallel preferential-flow channels
23	Nearly identical flow-parallel high-resistance and low-resistance patches	1	
24	Long-wavelength amorphous	8	K: Amorphous islands
25	Amorphous islands	2	
26	Islands surrounding scour holes	2	L: Islands with scour holes
27	Long-wavelength amorphous with deep scour holes	1	
28	Homogeneous low-resistance vegetation	8	M: Homogeneous low-resistance vegetation

predicted that high-resistance vegetation patches with total fractional coverage of at least 5% were most likely to evolve when autogenic peat accumulation rates were high, the initial coverage of high-resistance vegetation patches was high, and the equilibrium patch elevation was high relative to the water surface (Table S1). Of secondary importance were flow- and transport-related variables: high-resistance vegetation patches were more likely to evolve when high-flow periods were of short to medium duration, were not largely above the sediment entrainment threshold (i.e., when the interaction term between standardized and centered water-surface slope and critical bed shear stress for sediment entrainment was positive), and when high water-surface slopes were paired with low water depths or vice-versa (both of which result in moderate flow velocities (Harvey et al., 2009)).

4.3.2. Controls on patch and landscape morphology

Once high-resistance vegetation patches emerged and became stable, different environmental variables controlled different aspects of their morphology. To first order, Spearman's correlations (Fig. 3) revealed that water-surface slope, the initial aerial coverage of the high-resistance patches, and water depth were dominant controls on patch elongation, convolution of patch edges, and lacunarity (i.e., "gappiness") of the landscape. Meanwhile, intrinsic properties of the sediment (diffusivity under gravitational erosion) affected patch elongation relative to the flow direction, and vegetation (lateral propagation rate and community equilibrium elevation) affected number of patches, patch elongation, and landscape lacunarity. Landscapes with highly diffusive sediment tended to evolve patches that were wide in the direction normal to flow. In contrast, landscapes that had rapid lateral propagation of high-resistance vegetation communities tended to develop patches that were longer in the direction parallel to flow, with a lower edge density for the high-resistance patches. Thus, the dominant mechanism for the spreading of high-resistance vegetation patches had an impact on the orientation of patches relative to flow.

A discriminant analysis between the 12 different general classes of landscape pattern in which high-resistance patches evolved was significant at the $P = 0.019$ level (Hotelling–Lawley test). The first two discriminant axes (Table S2) cumulatively explained 49% of the variance in the dataset. Discriminant axis *1* was positive when the water-surface slope (positively related to flow velocities), sediment supply, and sediment entrainment threshold were relatively high. High values of the interaction term between the initial high-resistance patch coverage and sediment diffusivity on the high-resistance patches also contributed to positive values of the first discriminant score. This interaction term was related to the tendency for a moderate number of nascent patches to become stabilized at the beginning of the simulation. Positive values along the second discriminant axis corresponded to high water depths, low high-resistance vegetation patches relative to water level, supply-limited conditions, low sediment diffusivity in the low-resistance regions, and a relatively low high-resistance patch growth rate through autogenic peat accumulation and vegetative propagation.

Landscapes clustered in quadrant I of the discriminant space (Fig. 6A) were dominated by allogenic processes, driven by high flow velocities and high water levels, relative to the autogenic processes and gravitational erosion that typically cause high-resistance patch expansion. Nearly all landscapes with a distinctive anisotropic pattern structure were found in this quadrant. However, this dominance by flow was not a requirement for formation of an anisotropic pattern structure; large-scale, perpendicularly banded landscapes were found at the opposite extreme of the discriminant axes (quadrant III), indicating that there is no one mechanism through which interactions between flow, sediment transport, and vegetation cause emergence of anisotropically patterned wetlands.

Landscapes with long wavelengths of patch occurrence predominantly occupied the extreme of quadrant II, characterized by high water levels and low flow velocities. In contrast, maze-like, generally amorphous landscapes but with some flow-parallel or perpendicular anisotropy were found in the opposite quadrant (IV), where flow velocities were high but water levels low and/or the propensity for patch expansion high. These landscapes constituted an intermediate between the regularly patterned and amorphous wetlands, resulting from their position along a multi-dimensional continuum of the relative influences of transport processes, water level, and vegetation dynamics.

Interestingly, landscapes exhibiting pattern features aligned parallel and perpendicular to the flow (the "dual-orientation" landscapes) did not fall on a continuum between the flow-perpendicular and flow-

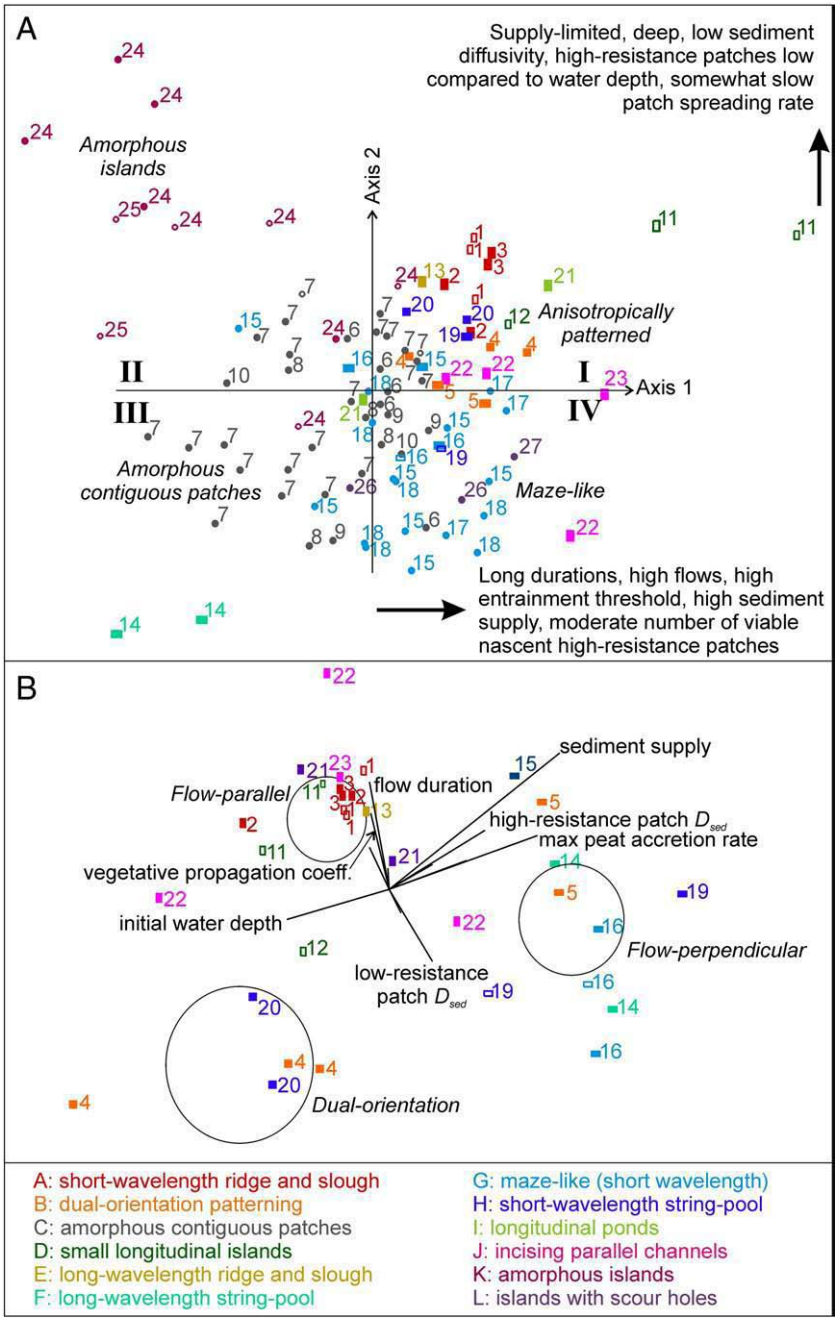

Fig. 6. Locations of RASCAL model outcomes in discriminant space. In A, the discriminant analysis maximizes the separation between general categories of simulation outcomes, shown in different colors that reference the category letters at the bottom of the figure. Specific categories (Table 4) are denoted by point numbers. Roman numerals denote quadrants. In B, a separate discriminant analysis maximizes the separation between patches with a dominant flow-parallel (tall rectangles), flow-perpendicular (horizontal rectangles), or dual-directional (squares) orientation. Circles indicate the centroid of each group. Only the most significant biplot rays in B are labeled, but values of all discriminant coefficients for A and B are available in Table S2.

parallel end-members (Fig. 6B). Dual-orientation landscapes had higher water depths and were more supply-limited than the flow-parallel or flow-perpendicular patterned wetlands. Perpendicularly patterned landscapes were the least supply-limited and had relatively short flow durations and relatively high sediment diffusivity in the low-resistance vegetation patches. In contrast, the salient features of the flow-parallel landscapes were relatively long flow durations and relatively high rates of vegetative propagation.

4.3.3. Controls on landscape stability

The configuration of landscape patches at early to middle stages of development did not predict whether it eventually stabilized in a highly heterogeneous combination of the high-resistance and low-resistance vegetation states. In other words, all classes of landscape outcomes contained members that stabilized and members that did not. Therefore, we analyzed controls on landscape stability independently of controls on landscape morphology.

To first order, variables that were correlated with measures of high-resistance vegetation abundance, coverage, and aggregation at the end of the simulation — all indicators of heterogeneous landscape stability — were the equilibrium elevation of the high-resistance vegetation patches and the degree of flow routing around high-resistance vegetation patches, indicated by the term $\max|\overline{u}_y|$ (see Fig. 3). Higher patch equilibrium elevations and lower degrees of flow routing around high-

resistance vegetation patches tended to result in more aggregated, aerially dominant high-resistance patches and less spatially cohesive low-resistance vegetation patches.

A discriminant analysis, significant at the $P = 0.017$ level (see Table S2), was consistent with these findings and provided additional insight. Namely, landscapes that stabilized in the highly heterogeneous configuration were also associated with higher water levels and a lower equilibrium elevation for high-resistance patches but had shorter flow pulse durations than landscapes that did not stabilize. The heterogeneous landscapes also tended to have higher sediment diffusivity in the high-resistance vegetation patches and lower sediment diffusivity in the low-resistance patches, both of which affect the shape of the topographic transition at patch edges.

4.4. Perturbations to trajectories of landscape evolution

When a long-wavelength, flow-parallel ridge and slough landscape that was approaching a heterogeneous equilibrium state was perturbed, the response to all perturbations examined was an accelerated lateral expansion of ridges (Fig. 7). The initial expansion was most rapid for perturbations that involved a 10 cm decrease in water depth. Following an instantaneous gain in coverage due to the exposure of new parts of the ridge/slough transition zone to high-resistance vegetation colonization, ridges continued to expand at the rate of 0.04% coverage per year. When water depth was the only environmental driver that was perturbed, subsequent expansion slowed to 0.005% coverage per year within 250 years of the perturbation, and the landscape eventually reached a new equilibrium at approximately 66% ridge coverage. Otherwise, landscape evolution trajectories continued to diverge to a nearly-homogeneous ridge state. A decrease in water-surface slope and increase in the resistance of slough vegetation also caused eventual divergence to a nearly-homogeneous landscape state, but at a slower rate (0.02% coverage per year).

We compared model predictions of ridge expansion under different types of perturbation to present-day rates of ridge expansion in a portion of the Everglades. Based on typical mean ridge dimensions of 522 m × 174 m (Larsen, 2008) and measured ridge expansion rates of 30 cm per year (P. McCormick, pers. comm., 2009), present-day ridge coverage in Loxahatchee National Wildlife Refuge is expanding at a rate of 0.08% per year, suggesting that this part of the Everglades, which has experienced curtailed flow velocities, is in the initial stages of degradation.

The type of perturbation affected not just the rate of ridge expansion but also the cross-sectional topography and patterns of erosion and deposition. In all cases, ridges expanded laterally as the high-resistance sawgrass stabilized new portions of ridge edges. When the sole perturbation was reduced water depth, expansion of ridges was accompanied by a steepening of the ridge/slough topographic transition and maintenance of high slough erosion rates and overall sediment redistribution (Fig. 8). In contrast, the ridge edge topographic transition became less steep when water-surface slope or vegetation were perturbed in a direction that resulted in lower flow velocities, causing erosion within sloughs to become more localized. The lowest slough erosion rates and ridge deposition rates occurred when water-surface slope was perturbed. When the slough vegetation composition was perturbed to a higher-resistance state, sediment redistribution was greater than when water-surface slope was perturbed, causing subtle differences in the shape of the topographic transition between ridges and sloughs. Lastly, when water depth was perturbed in concert with vegetation composition or water-surface slope, the tops of ridge patches became substantially more rounded.

4.5. Reversibility of perturbation trajectories

In general, perturbation trajectories were partially reversible (Fig. 9) only when newly-colonized parts of high-resistance vegetation patches remained at a low elevation (i.e., when patch edges were rounded) (Fig. 8). Under this circumstance, the low-resistance vegetation patch coverage could be recovered nearly to the pre-perturbation level by increasing water depth. The degree to which this recovery occurred depended on the shape of the patch edges prior to restoration of the pre-perturbation conditions.

The depth-only perturbation, in contrast, was not reversible by an increase in water level because of the nearly vertical topographic transitions that had evolved at the patch edges. Likewise, restoring pre-perturbation vegetation and water-surface slope to the other cases had little to no effect on patch coverage, though doing so did halt subsequent ridge expansion.

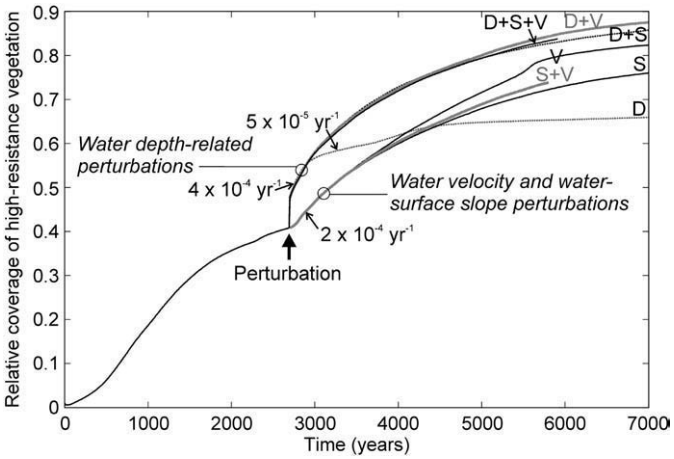

Fig. 7. Perturbation trajectories for a landscape that was initially approaching equilibrium. Perturbations, which occurred at 2700 years after initiation of landscape evolution (the age of the Everglades ridge and slough landscape (Willard and Cronin, 2007)) were various permutations of decreased water depth (D), decreased water-surface slope (S), and an increase in the density and vegetative drag of the low-resistance vegetation community due to invasion by high-resistance vegetation (V). Numbered arrows show rates of high-resistance patch expansion (units are relative coverage per year) at different regions of the perturbation trajectories.

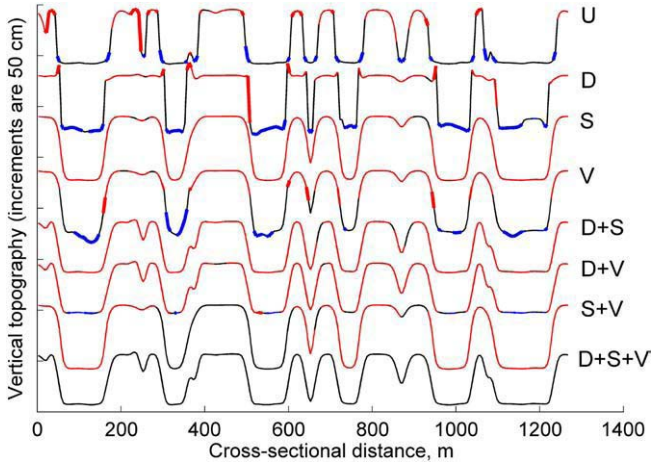

Fig. 8. Cross-sectional profiles across the unperturbed (U) landscape at 41% high-resistance vegetation coverage and perturbed landscapes at 60% high-resistance vegetation coverage. (D = decreased water depth, S = decreased water-surface slope, V = increased vegetative drag in low-resistance patches due to invasion by high-resistance vegetation.) Cross-sections are plotted with respect to an arbitrary datum for ease of viewing. Red and blue segments show zones of sediment deposition and erosion, respectively, where the thickness of the line is related to the magnitude of the bed sediment flux. Thin red and blue lines indicate immeasurably low rates of bed sediment flux.

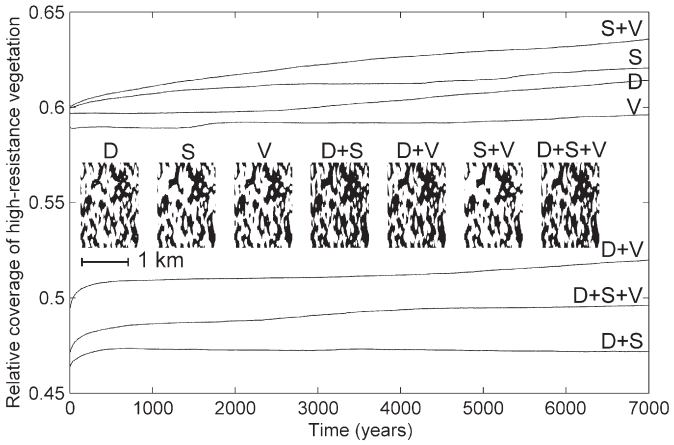

Fig. 9. Irreversibility of landscape perturbation trajectories. At time 0, the original perturbation to water depth (D), water-surface slope (S), or water depth (D) shown in Fig. 7 was reversed. The domain at time 0 was initialized as the topography for the corresponding perturbed case at a 60% high-resistance vegetation coverage. Planform views of vegetation state (white = high-resistance patch and black = low-resistance patch) at the end of the analysis are provided.

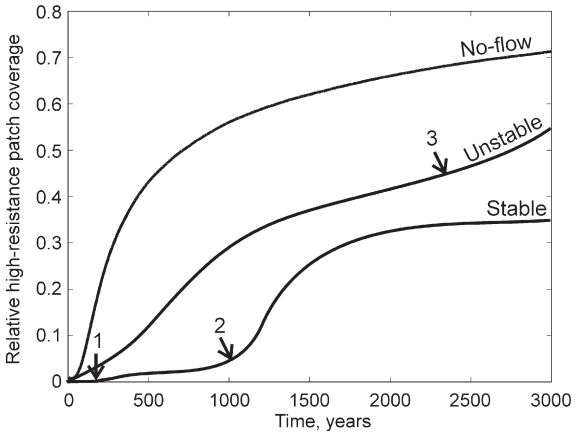

Fig. 10. Thresholds and stability of three types of landscapes experiencing high-resistance vegetation community expansion. Thresholds 1, 2, and 3 are all tipping points, beyond which the expansion of the high-resistance vegetation patch accelerates.

5. Discussion

5.1. Feedback among flow, vegetation, and sediment transport in wetlands

Although the landscape outputs of our cellular automata model have not yet undergone rigorous validation, the model leads to an improved mechanistic understanding of the emergent properties that can arise from interactions among flow, vegetation, and sediment transport in ecosystems where the simulated processes are dominant. Overall, our model suggests that the effects of these interactions are highly nonlinear, characterized by thresholds and positive and negative feedbacks. As landscapes evolve from a relatively low-flow-resistance state, vegetation patches initially develop gradually, largely through vegetative propagation, autogenic peat accumulation, and low-level sediment deposition. At these early stages of patch development, the nascent high-resistance patches are susceptible to loss or delayed growth if the diffusivity of the sediment is high, flow and sediment transport are low (or, conversely, if local flow velocities are high and stochastic vegetation death leads to erosion and loss of the patch) and/or high water depths stunt the growth of vegetation. Sometimes these processes can cause the landscape to remain predominantly low-resistance vegetation. However, once a threshold of patch growth (which can be as low as a fraction of 1% high-resistance vegetation coverage; see arrow 1 of Fig. 10) is attained, high-resistance patches begin to develop rapidly through positive feedback.

The positive feedback that causes initial rapid patch growth is largely due to autogenic peat accretion, since this growth also occurs under no-flow conditions (Fig. 10). Over a range of local soil elevations relative to water depth, increases in soil elevation result in a faster accumulation of peat (Larsen et al., 2007). This rapid gain in soil elevation results in increased vegetation productivity and increased patch expansion through vegetative propagation and gravitationally driven erosion, which has a diffusive effect on topography. However, when flow velocities are high and high-resistance patch coverage is small (<5%), the positive-feedback gain in aerial patch coverage can be halted (e.g., Fig. 10) until more patches are established by macrophytes stabilizing sediment deposits. As more deposits are established, more flow is routed around the high-resistance vegetation patches, causing increased redistribution of sediment, which ultimately results in substantial deposition in the lee of the nascent patches, contributing to their elongation and area. Landscapes that experience this second threshold-type response early in their evolution tend to evolve narrow but elongated high-resistance vegetation patches oriented parallel to flow.

Once high-resistance patches grow to be shallower than the optimum depth for peat accumulation, their vertical and lateral growth through vegetation processes slows. A negative autogenic peat accretion feedback (Larsen et al., 2007) then maintains an equilibrium patch elevation. However, because of gravitational erosion, patches can continue to expand, and in landscapes where the sediment diffusivity is high and flow velocities are relatively low, the landscape diverges to a more homogenous high-resistance vegetation state. Otherwise, flow erodes sediment from the edges of the high-resistance vegetation patches, counterbalancing the additions of sediment to this region from higher portions of the patch and stabilizing the shape of the patch. Some of this sediment is redistributed to high-resistance patches further downstream, just to the interior of the vegetation boundary (Fig. 8). In fact, high-resistance vegetation patches that remain low relative to the water surface characterize many landscapes that stabilized (Fig. 6B). Thus, two negative feedback processes, autogenically and allogenically driven, maintained equilibrium in the vertical and lateral dimensions, respectively, of some landscapes.

Some landscapes passed through another threshold (arrow 3 of Fig. 10) and experienced positive-feedback growth of high-resistance vegetation patches once they had begun to stabilize through the negative feedbacks discussed above. This positive-feedback response was always associated with the formation of narrow preferential-flow channels (e.g., Fig. 1). Preferential-flow channels would form when lower portions of the low-resistance patches consistently experienced greater flow and erosion than surrounding parts of the low-resistance patches, causing incision and promoting a positive-feedback deepening and lengthening of the channels. Because of the water balance, as flow velocities and depth increased in the preferential-flow channels, the regional water level declined, exposing new portions of the high-resistance patch edges to high-resistance vegetation colonization. This feedback is similar to the feedback that forms narrow parallel tidal channels in marshes that develop on tidal flats (Temmerman et al., 2007).

Because of preferential channel formation, surface-flow wetlands that have a highly heterogeneous equilibrium are relatively uncommon. They must experience flow fast enough to redistribute sediment across the landscape but not so fast that there is large variance in erosion rates within the low-resistance patches. It is because of this preferential erosion of low-resistance vegetation patches that water-surface slope and flow pulse duration have a positive effect on final

topographic range (an indicator of preferential channel incision), while the sediment entrainment threshold has a negative effect (Fig. 3).

Feedback between preferential low-resistance patch erosion and autogenic and allogenic high-resistance patch expansion also likely governs the orientation of landscape pattern structures. All anisotropic pattern structures require relatively high flow velocities; orientations are more influenced by the sediment supply, flow pulse duration, and dominant mode of high-resistance patch expansion. When the sediment supply is low and flow duration long, low-resistance patches erode most evenly. In contrast, when sediment supply is large but flow pulse durations are short (true for the perpendicularly patterned landscapes), low-resistance patches have a greater potential for preferential erosion, and deposition zones can shift to elevations lower along the patch transition (e.g., Fig. 8, case V), contributing to patch expansion perpendicular to the slope. Initial instabilities thus cause the landscape to develop into perpendicular strings of vegetation interspersed among deep pools.

Regular pattern formation perpendicular to the flow is further reinforced when the dominant mode of high-resistance patch expansion is erosive rather than vegetative processes. As is apparent from Eq. (7), ridge spreading through erosive processes occurs most rapidly when the elevations of high-resistance patches are great. In environments where vegetation growth is slow, the deposition of sediment on emerging high-resistance patch surfaces is needed for these patches to accrete vertically, become permanent, and begin expanding. Thus, high-resistance vegetation just downstream of a source area for suspended sediment (i.e., low-resistance patch) is most likely to become permanent, and merging of high-resistance patches in a direction parallel to flow is unlikely, contributing to the development of perpendicular patterning.

Landscapes patterned parallel to flow experience the most sediment redistribution, with the longest flow pulse durations and low to moderate sediment supply, resulting in low-resistance patches that erode relatively evenly. Sediment deposition occurs at relatively high elevations along patch transitions (Fig. 8, case U), which, along with low sediment diffusivity, keeps high-resistance patches narrow and steep-sided. However, high vegetative propagation rates, which lead to net patch expansion only along edges that are not being actively eroded, are needed to contribute to patch elongation parallel to flow. Rapid stabilization of sediment deposited in the lee of nascent high-resistance patches by vegetation and subsequent vertical accretion and horizontal propagation contribute to the merging of high-resistance patches in a direction parallel to flow.

Dual-orientation landscapes, like perpendicularly patterned landscapes, arise from relatively short flow pulses, but low sediment supply ensures that low-resistance patches erode evenly. Still, because of relatively short flow durations, patch expansion rates are relatively large compared to sediment redistribution rates. High water depths, however, prevent universal expansion of the high-resistance patches. The net result is that because of an initial instability due to the stochasticity of sediment transport, high-resistance patches expand parallel to the slope in some locations and perpendicular to the slope in other locations. Patches that expand perpendicular to the slope effect a topographic steering of the flow that maintains patch expansion in the perpendicular direction. Meanwhile, high water depths and low-level scour maintain disconnected but regularly spaced low-resistance vegetation patches.

5.2. Universality and uniqueness of feedbacks affecting landscape patterning

The landscape types predicted to emerge from feedback among flow, sediment transport, and vegetation growth are similar to other maze-like, flow-parallel, flow-perpendicular, and dual-patterned wetland landscapes found throughout the world (Fig. 1). However, RASCAL provides the first explanation of how a sediment transport feedback can instigate and govern formation of these patterns. These pattern structures are also recognized to emerge from other combinations of feedback processes. The processes described to result in patterning, alone or in concert, include differential peat accretion as a function of local water level and vegetation community (included in our model; (Nungesser, 2003)), a water ponding mechanism in which water ponds behind hummocks of vegetation that have low hydraulic conductivity (Swanson and Grigal, 1988; Couwenberg and Joosten, 2005), and a nutrient accumulation mechanism whereby transpiring patches of high-productivity vegetation concentrate nutrients in the subsurface and initiate a scale-dependent feedback (Rietkerk et al., 2004b; Eppinga et al., 2008).

Eppinga et al. (2009b) used modeling in a factorial design experiment to show how different combinations of the feedback processes described above (except for sediment transport) produce different wetland pattern structures in flat or sloping boreal peatlands given an initial instability. Despite differences in vegetation community and the degree of submergence of high-resistance patches between RASCAL and Eppinga et al.'s model, results were remarkably consistent. At low water-surface slopes, where little sediment is transported, generally amorphous patterns resulted, similar to predictions of the Eppinga et al. model on flat ground with the peat accumulation and water ponding mechanisms turned on. When water-surface slopes were higher but flow pulse durations were not long enough to cause much sediment redistribution, strings of high-resistance vegetation formed parallel to the slope in both RASCAL and the Eppinga et al. model on a sloping surface with the peat accumulation mechanism turned on. When water ponding was also turned on, the Eppinga et al. model predicted a dual-orientation pattern to form, consistent with RASCAL for high water level (but still short flow duration) conditions. For maze-like (on flat ground) or sharply delineated perpendicular string-pool sequences or parallel ridges (on slopes) to develop, Eppinga et al. predicted that a nutrient accumulation feedback was needed. Our results show that, alternatively, a sediment transport feedback can produce these patterns. Synthesizing, these well-defined patterns require a limiting resource for vegetation growth (nutrients or soil elevation) and feedback among vegetation, peat accumulation, and water level. Even in bogs where nutrient limitation is a dominant driver, low-level sediment transport by flowing water may provide a previously unrecognized explanation of the cause of the initial topographic instability that triggers landscape-scale pattern development.

5.3. Stability and metastability of landscape pattern and implications for wetland restoration

Patterned landscapes worldwide are known to be relatively low-entropy systems that reside in thermodynamic local minima and, given a large enough perturbation, undergo catastrophic and often irreversible shifts to a more homogeneous and more stable equilibrium (Rietkerk et al., 2004a; Eppinga et al., 2009a,b). Our model experiments provide additional support for this concept of wetland metastability, showing for the first time that wetlands oriented parallel to flow also exhibit this characteristic. Namely, perturbations to flow velocity that cause high-resistance vegetation to expand cannot be reversed by restoring the pre-perturbation flow velocity because the presence of that vegetation suppresses erosion. Vegetation expansion can only be reversed by reducing the abundance of high-resistance vegetation prior to restoring the flows needed to halt subsequent patch expansion (Fig. 9). The cross-sectional shape of patch edges is an indicator of the potential for patterned landscape restoration through a combination of increased flow velocities and water levels, as well as a coarse indicator of the type of perturbation that has already impacted landscape evolution (Fig. 8). Landscapes with the greatest potential for reversal of high-resistance patch

expansion are those with rounded ridges, where emergent vegetation at the edge is subject to drowning with increases in water depth.

It is a unique feature of wetland evolution that perturbations to flow velocity (through perturbations to water-surface slope or low-resistance vegetation community composition) have an effect independent of perturbations to water depth. In rivers, these effects are correlated, since depth is a dominant driver of flow velocity. However, in wetlands where vegetative resistance elements protrude through the water column, water depth primarily controls vegetation colonization and vertical peat accretion rates, whereas water-surface slope and vegetation community composition are the dominant controls on flow velocities and hence, sediment transport (Harvey et al., 2009).

Our perturbation/restoration model results are consistent with the past behavior of the Everglades ridge and slough landscape, which experienced ridge expansion during climatically dry periods and subsequent contraction during wet periods (Bernhardt and Willard, 2009). RASCAL suggests that the much more rapid expansion of ridges that has occurred over the last century (Willard and Cronin, 2007) may be slowed or even partially reversed by increasing water depths. However, a combination of increased flow velocities, greater average water depths, and removal of high-flow-resistance vegetation by drowning or other mechanisms will likely be needed to restore slough connectivity and halt future ridge expansion.

It is noteworthy that while truly metastable heterogeneous wetlands are somewhat rare, quasi-metastable patterned wetlands are likely common. The distinction between the two is that quasi-metastable wetlands are those that would eventually pass through the preferential channel formation threshold and undergo rapid high-resistance patch expansion (e.g., Fig. 10). However, before that threshold is reached, high-resistance patches expand at a potentially immeasurably small rate. In reality, episodic, extreme events that "reset" the system (e.g., floods, fires, windstorms) may displace these landscapes backwards on their evolution trajectories before the preferential channel formation threshold is reached. Thus, it was important to consider the driving factors producing landscape stability separately from those producing particular landscape morphologies.

Because of the metastable nature of heterogeneously vegetated wetlands, it is not possible to produce a single "channel pattern stability diagram" that predicts wetland morphology over a range of environmental drivers without taking into consideration the antecedent vegetation composition. However, our analyses (particularly Figs. 3 and 6) provide guidance for wetland landscape pattern prediction given a low-resistance initial condition and yields additional hypotheses about new driving mechanisms of landscape patterning that should be subjected to field testing. One application of the improved understanding of the dynamics of flow/vegetation/sediment feedbacks that RASCAL provides lies in designing and constructing wetlands for habitat provision or water treatment. Different regions of the discriminant parameter space (Fig. 6A and B) clearly separated wetlands with different degrees of heterogeneity, patch cohesion, and edge distribution – all variables that affect habitat (Wang et al., 2008). Because relatively high throughput is a requirement for most treatment wetlands, most of these systems would fall on the right side of the discriminant space, where flow velocities and sediment transport are relatively high. Under these conditions, preferential channel formation that results in a higher variance in water residence time and lower treatment efficiency is often inevitable (see also Lightbody et al., 2008), but the spatial arrangement of that heterogeneity can improve or inhibit treatment efficiency (Worman and Kronnas, 2005). For instance, transverse deep zones, similar to those of wetland class F, can improve wetland performance (Lightbody et al., 2007), whereas connected preferential-flow channels would be undesirable. Using our analysis and the RASCAL model as a guide, these and other wetlands can be designed to be self-sustaining at optimum efficiency.

6. Conclusions

Our cellular automata model suggests that several key characteristics govern the dynamical effects of interactions among flow, vegetation, and sediment transport in floodplains and wetlands:

- The relative influence of autogenic (i.e., *in situ* peat accretion) versus allogenic (i.e., sediment transport) processes is the dominant factor determining the general class of pattern that emerges.
- Among allogenic processes, the magnitude and duration of flow pulses that transport sediment have a dominant influence on whether regular, anisotropic patterns form and the direction of pattern orientation. In general, highly structured anisotropic patterns form when the wetland experiences long, high-velocity flow pulses that transport sediment.
- The elevation of high-resistance patches with respect to water level influences how rapidly patches expand via vegetative propagation, the extent to which they can serve as a sink for suspended sediment as a result of redistribution by flow, and the extent to which they cause topographic steering of flow. As a result, both patch stability and the development of dual-directional landscape patterns are highly sensitive to changes in water level.
- The dominant mechanism by which high-flow-resistance patches dominantly expand affects not only relative coverage of high-flow-resistance vegetation, but also the shape of the topographic transition at patch edges and whether nascent patches in close proximity to established patches can become permanent and/or merge with other patches. The shape of the edge gradient ultimately influences landscape evolution through its effects on patterns of sediment redistribution at patch edges, patch orientation with respect to flow, and the reversibility of patch expansion. Likewise, the establishment and merging of nascent patches impacts the orientation and wavelength of the landscape.
- The spatial variability of erosion rates within low-flow-resistance patches is an allogenic metric that governs high-resistance patch expansion at late stages of landscape evolution through its influence on preferential channel formation. When low-resistance patches erode at a spatially variable rate, narrow preferential channels form, and high-resistance patches become wide.
- Antecedent vegetation distribution and topographic variability are important in governing future landscape evolution, due to hysteresis caused by feedback among vegetation, flow, and sediment transport. These characteristics influence the reversibility of perturbations and potential for landscape restoration.
- Our modeling suggests that loss of the ridge and slough landscape over the past century was driven most rapidly by declining water levels, with decreases in flow velocity affecting the system over longer time scales. Also, once the flow resistance of channels (e.g., Everglades sloughs) has increased sufficiently, restoration of historic water depths and flow velocities can no longer halt further ridge expansion. Reducing ridge coverage will require maintenance of high water levels, increased flow velocity, and, in many locations, thinning of slough vegetation to reduce flow resistance.

Predicting the relative importance of these characteristics or the influence of environmental variables on overall landscape pattern is complicated by highly nonlinear interactions among these processes and variables. Our model suggests that floodplain and wetland landscape morphology is sensitive to many driving variables, even when processes such as nutrient limitation and species succession are excluded. However, when the driving variables that we examined were collapsed into two discriminant scores, reasonably good separation between landscape pattern types was achieved, providing a rough predictive tool. These results were also qualitatively consistent with wetland pattern types worldwide and with other theoretical analyses and generate hypotheses about landscape pattern generation and stability to be tested in the field. Given the high

natural variability in wetland sediment properties, flows, and wetland vegetation species composition and productivity, site-specific modeling will for some time remain the best predictive tool for wetland evolution. The relative simplicity and efficiency of RASCAL, combined with its modularized nature, make it readily adaptable and suitable for coupling to other models simulating nutrient transport or detailed vegetation dynamics. In this way, it provides an ideal tool for predicting how wetland landscape pattern and associated ecosystem services will respond to climate change, urban development, or restoration attempts.

Acknowledgements

Support for this study was provided by the USGS National Research Program, USGS Priority Ecosystems Science Program, NSF grant EAR-0732211, and the National Park Service through interagency agreement F5284-08-0024. We are grateful to Morgan Franklin for comments and help with figure preparation and analysis and to Kristopher Larsen for help with figure preparation. The manuscript benefited from thorough reviews and stimulating ideas by Maarten Eppinga, Waite Osterkamp, Lisamarie Windham-Myers, and an anonymous referee. Use of trade or product names is for descriptive purposes only and does not constitute endorsement by the USGS.

Appendix A. Supplementary data

Supplementary data associated with this article can be found, in the online version, at doi:10.1016/j.geomorph.2010.03.015.

References

ASCE (American Society of Civil Engineers), 2008. The U.S. Waterway System - Transportation Facts, Navigation Data Center. U.S. Army Corps of Engineers, Alexandria, VA.

Bays, J.S., Knight, R.L., 2002. Fort Deposit constructed treatment wetlands system: 10-year review. In: Pries, J. (Ed.), Treatment Wetlands for Water Quality Improvement: Quebec 2000 Conference Proceedings. Pandora Press, pp. 35–44.

Bazante, J., Jacobi, G., Solo-Gabriele, H., Reed, D., Mitchell-Bruker, S., Childers, D., Leonard, L., Ross, M., 2006. Hydrologic measurements and implications for tree island formation within Everglades National Park. J. Hydrol. 329, 606–619.

Beisner, B.E., Haydon, D.T., Cuddington, K., 2003. Alternative stable states in ecology. Front. Ecol. Environ. 1, 376–382.

Bernhardt, C.E., Willard, D.A., 2009. Response of the Everglades' ridge and slough landscape to late Holocene climate variability and 20th century water-management practices. Ecol. Appl. 19, 1723–1738.

Bridgham, S.D., Megonigal, J.P., Keller, J.K., Bliss, N.B., Trettin, C., 2006. The carbon balance of North American wetlands. Wetlands 26, 889–916.

Brinson, M.M., 1993. A Hydrogeomorphic Classification for Wetlands, Wetlands Research Technical Report WRP-DE-4. Army Corps of Engineers, Washington, DC.

Chmura, G.L., Anisfeld, S.C., Cahoon, D.R., Lynch, J.C., 2003. Global carbon sequestration in tidal, saline wetland soils. Glob. Biogeochem. Cycles 17, 1111. doi:10.1029/2002GB001917.

Christiansen, T., Wiberg, P.L., Milligan, T.G., 2000. Flow and sediment transport on a tidal salt marsh surface. Estuar. Coast. Shelf S. 50, 315–331.

Couwenberg, J., Joosten, H., 2005. Self-organization in raised bog patterning: the origin of microtope zonation and mesotope diversity. J. Ecol. 93, 1238–1248.

D'Alpaos, A., Lanzoni, S., Marani, M., Rinaldo, A., 2007. Landscape evolution in tidal embayments: modeling the interplay of erosion, sedimentation, and vegetation dynamics. J. Geophys. Res. 112. doi:10.1029/2006JF000537.

DeBusk, W.F., Reddy, K.R., 1998. Turnover of detrital organic carbon in a nutrient-impacted Everglades marsh. Soil Sci. Soc. Am. J. 62, 1460–1468.

Doeschl-Wilson, A.B., Ashmore, P.E., 2005. Assessing a numerical cellular braided-stream model with a physical model. Earth Surf. Process. Land. 30, 519–540.

Duan, J., Wiggins, S., 1997. Lagrangian transport and chaos in the near wake of the flow around an obstacle: a numerical implementation of lobe dynamics. Nonlin. Proc. Geophys. 4, 125–136.

Eppinga, M., Rietkerk, M., Borren, W., Lapshina, E., Bleuten, W., Wassen, M., 2008. Regular surface patterning of peatlands: confronting theory with field data. Ecosystems 11, 520–536.

Eppinga, M.B., Rietkerk, M., Wassen, M.J., de Ruiter, P.C., 2009a. Linking habitat modification to catastrophic shifts and vegetation patterns in bogs. Plant Ecol. 200, 53–68.

Eppinga, M.B., de Ruiter, P.C., Wassen, M.J., Rietkerk, M., 2009b. Nutrients and hydrology indicate the driving mechanisms of peatland surface patterning. Am. Nat. 173, 803–818.

Fennema, R.J., Neidrauer, C.J., Johnson, R.A., MacVicar, T.K., Perkins, W.A., 1994. A computer model to simulate natural Everglades hydrology. In: Davis, S.M., Ogden, J.C. (Eds.), Everglades: The Ecosystem and Its Restoration. St. Lucie Press, Boca Raton, FL, pp. 249–289.

FitzGerald, D.M., Fenster, M.S., Argow, B.A., Buynevich, I.V., 2008. Coastal impacts due to sea-level rise. Annu. Rev. Earth Planet. Sci. 36, 601–647.

Fonstad, M.A., 2006. Cellular automata as analysis and synthesis engines at the geomorphology–ecology interface. Geomorphology 77, 217–234.

French, J.R., Stoddart, D.R., 1992. Hydrodynamics of salt marsh creek systems: implications for marsh morphological development and material exchange. Earth Surf. Process. Land. 17, 235–252.

Garcia, M.H. (Ed.), 2007. Sedimentation engineering: processes, management, modeling, and practice. ASCE Publications, Alexandria, VA. 1132 pp.

German, E.R., 2000. Regional evaluation of evapotranspiration in the Everglades. U.S. Geological Survey Water-Resources Investigations Report 00-4217, Tallahassee, Florida. 48 pp.

Givnish, T.J., Volin, J.C., Owen, V.D., Volin, V.C., Muss, J.D., Glaser, P.H., 2008. Vegetation differentiation in the patterned landscape of the central Everglades: importance of local and landscape drivers. Global Ecol. Biogeogr. 17, 384–402.

Gleason, P.L., Stone, P., 1994. Age, origin, and landscape evolution of the Everglades peatland. In: Davis, S.M., Ogden, J.C. (Eds.), Everglades: The Ecosystem and Its Restoration. St. Lucie Press, Boca Raton, FL, pp. 149–197.

Harvey, J.W., McCormick, P.V., 2009. Groundwater's significance to changing hydrology, water chemistry, and biological communities of a floodplain ecosystem, Everglades, South Florida, USA. Hydrogeol. J. 17, 185–201.

Harvey, J.W., Krupa, S.L., Krest, J.M., 2004. Ground water recharge and discharge in the central Everglades. Ground Water 42, 1090–1102.

Harvey, J.W., Schaffranek, R.W., Noe, G.B., Larsen, L.G., Nowacki, D., O'Connor, B.L., 2009. Hydroecological factors governing surface-water flow on a low-gradient floodplain. Water Resour. Res. 45, W03421. doi:10.1029/2008WR007129.

Huang, H.Q., Nanson, G.C., 2007. Why some alluvial rivers develop an anabranching pattern. Water Resour. Res. 43. doi:10.1029/2006WR005223.

Hupp, C.R., Osterkamp, W.R., 1996. Riparian vegetation and fluvial geomorphic processes. Geomorphology 14, 277–295.

Iman, R.L., Helton, J.C., Campbell, J.E., 1981. An approach to sensitivity analysis of computer models. Part 1. Introduction, input variable selection and preliminary variable assessment. J. Qual. Technol. 13, 174–183.

Istanbulluoglu, E., Bras, R.L., 2005. Vegetation-modulated landscape evolution: effects of vegetation on landscape processes, drainage density, and topography. J. Geophys. Res. 110, F02012. doi:10.1029/2004/JF000249.

Kirwan, M.L., Murray, A.B., 2007. A coupled geomorphic and ecological model of tidal marsh evolution. Proc. Natl. Acad. Sci. 104, 6118–6122.

Krest, J.M., Harvey, J.W., 2003. Using natural distributions of short-lived radium isotopes to quantify groundwater discharge and recharge. Limnol. Oceanogr. 48, 290–298.

Larsen, L.G., 2008. Hydroecological feedback processes governing self-organization of the Everglades ridge and slough landscape. Ph.D Thesis, University of Colorado. Boulder.

Larsen, L.G., Harvey, J.W., Crimaldi, J.P., 2007. A delicate balance: ecohydrological feedbacks governing landscape morphology in a lotic peatland. Ecol. Monogr. 77 (4), 591–614.

Larsen, L.G., Harvey, J.W., Crimaldi, J.P., 2009a. Morphologic and transport properties of natural organic floc. Water Resour. Res. 45, W01410. doi:10.1029/2008WR006990.

Larsen, L.G., Harvey, J.W., Noe, G.B., Crimaldi, J.P., 2009b. Predicting organic floc transport dynamics in shallow aquatic ecosystems: Insights from the field, the laboratory, and numerical modeling. Water Resour. Res. 45, W01411. doi:10.1029/2008WR007221.

Larsen, L.G., Harvey, J.W., Crimaldi, J.P., 2009c. Predicting bed shear stress and its role in sediment dynamics and restoration potential of the Everglades and other vegetated flow systems. Ecol. Eng. 35, 1773–1785.

Lee, J.K., Roig, L.C., Jenter, H.L., Visser, H.M., 2004. Drag coefficients for modeling flow through emergent vegetation in the Florida Everglades. Ecol. Eng. 22, 237–248.

Leonard, L.A., Luther, M.E., 1995. Flow hydrodynamics in tidal marsh canopies. Limnol. Oceanogr. 40, 1474–1484.

Leonard, L.A., Reed, D.J., 2002. Hydrodynamics and sediment transport through tidal marsh canopies. J. Coast. Res. 36, 459–469.

Lightbody, A.F., Nepf, H.M., 2006a. Prediction of near-field shear dispersion in an emergent canopy with heterogeneous morphology. Environ. Fluid Mech. 6, 477–488.

Lightbody, A.F., Nepf, H.M., 2006b. Prediction of velocity profiles and longitudinal dispersion in emergent salt marsh vegetation. Limnol. Oceanogr. 51, 218–228.

Lightbody, A.F., Nepf, H.M., Bays, J.S., 2007. Mixing in deep zones within constructed treatment wetlands. Ecol. Eng. 29, 209–220.

Lightbody, A.F., Avener, M.E., Nepf, H.M., 2008. Observations of short-circuiting flow paths within a free-surface wetland in Augusta, Georgia, USA. Limnol. Oceanogr. 53, 1040–1053.

Marshall III, F.E., Wingard, G.L., Pitts, P., 2009. A simulation of historic hydrology and salinity in Everglades National Park: coupling paleoecologic assemblage data with regression models. Estuar. Coast. 32, 37–53.

McGarigal, K., Cushman, S.A., Neel, M.C., Ene, E., 2002. FRAGSTATS: Spatial Pattern Analysis Program for Categorical Maps. Computer software program produced by the authors at the University of Massachusetts, Amherst. Available www.umass.edu/landeco/research/fragstats/fragstats.htm.

Mertes, L.A.K., Daniel, D.L., Melack, J.M., Nelson, B., Martinelli, L.A., Forsberg, B.R., 1995. Spatial patterns of hydrology, geomorphology, and vegetation on the floodplain of the Amazon River in Brazil from a remote sensing perspective. Geomorphology 13, 215–232.

Miao, S.L., Sklar, F.H., 1998. Biomass and nutrient allocation of sawgrass and cattail along a nutrient gradient in the Florida Everglades. Wetlands Ecol. Manage. 5, 245–263.

Millar, R.G., 2000. Influence of bank vegetation on alluvial channel patterns. Water Resour. Res. 36, 1109–1118.
Millennium Ecosystem Assessment, 2005. Ecosystems and Human Well-being: Wetlands and Water Synthesis. World Resources Institute, Washington, D.C.
Morris, J.T., Sundareshwar, P.V., Nietch, C.T., Kjerfve, B., Cahoon, D.R., 2002. Responses of coastal wetlands to rising sea-level. Ecology 83, 2869–2877.
Murray, A.B., Paola, C., 2002. A cellular model of braided rivers. Nature 371, 54–57.
Murray, A.B., Paola, C., 2003. Modelling the effect of vegetation on channel pattern in bedload rivers. Earth Surf. Process. Land. 28, 131–143.
Myers, R.D., 1999. Hydraulic properties of South Florida wetland peats. M. Eng. Thesis, University of Florida, Gainesville, FL.
National Research Council, 2003. Does water flow influence Everglades landscape patterns? National Academies Press, Washington, DC. 41 pp.
Nepf, H.M., 1999. Drag, turbulence, and diffusion in flow through emergent vegetation. Water Resour. Res. 35, 479–489.
Nepf, H.M., 2004. Vegetated flow dynamics. In: Fagherazzi, S., Marani, M., Blum, L.K. (Eds.), The Ecogeomorphology of Tidal Marshes. American Geophysical Union, Washington, DC, pp. 137–163.
Nepf, H., Sullivan, J., Zavistoski, R., 1997. A model for diffusion within emergent vegetation. Limnol. Oceanogr. 42, 85–95.
Neumeier, U., Ciavola, P., 2004. Flow resistance and associated sedimentary processes in a *Spartina maritima* salt-marsh. J. Coastal Res. 20, 435–557.
Nungesser, M.K., 2003. Modelling microtopography in boreal peatlands: hummocks and hollows. Ecol. Model. 165, 175–207.
Ogden, J.C., 2005. Everglades ridge and slough conceptual ecological model. Wetlands 25, 810–820.
Parsons, J.A., Fonstad, M.A., 2007. A cellular automata model of surface water flow. Hydrol. Process. 21, 2189–2195.
Pasternack, G.B., Brush, G.S., Hilgartner, W.B., 2001. Impact of historic land-use change on sediment delivery to a Chesapeake Bay subestuarine delta. Earth Surf. Process. Land. 26, 407–427.
Pope, S.B., 2000. Turbulent Flows. Cambridge University Press, Cambridge. 769 pp.
Rietkerk, M., Dekker, S.C., de Ruiter, P.C., van de Koppel, J., 2004a. Self-organized patchiness and catastrophic shifts in ecosystems. Science 305, 1926–1929.
Rietkerk, M., Dekker, S.C., Wassen, M.J., Verkroost, A.W.M., Bierkens, M.F.P., 2004b. A putative mechanism for bog patterning. Am. Nat. 163 (5), 699–708.
Saiers, J.E., Harvey, J.W., Mylon, S.E., 2003. Surface-water transport of suspended matter through wetland vegetation of the Florida everglades. Geophys. Res. Lett. 30 (19) HLS 3-1 - HLS 3-5.
Sartoris, J.J., Thullen, J.S., Barber, L.B., Salas, D.E., 1999. Investigation of nitrogen transformations in a southern California constructed wastewater treatment wetland. Ecol. Eng. 14, 49–65.
Schumm, S.A., 1985. Patterns of alluvial rivers. Annu. Rev. Earth Planet. Sci. 13, 5–27.
Suding, K.N., Gross, K.L., Houseman, G.R., 2004. Alternative states and positive feedbacks in restoration ecology. Trends Ecol. Evol. 19, 46–53.
Swanson, D.K., Grigal, D.F., 1988. A simulation model of mire patterning. Oikos 53, 309–314.
Tal, M., Paola, C., 2007. Dynamic single-thread channels maintained by the interaction of flow and vegetation. Geology 35, 347–350.
Tal, M., Gran, K., Murray, A.B., Paola, C., Hicks, D.M., 2004. Riparian vegetation as a primary control on channel characteristics in multi-thread rivers. In: Bennett, S.J., Simon, A. (Eds.), Riparian Vegetation and Fluvial Geomorphology. American Geophysical Union, Washington, D.C., pp. 43–58.
Temmerman, S., Bouma, T.J., Govers, G., Wang, Z.B., De Vries, M.B., Herman, P.M.J., 2005. Impact of vegetation on flow routing and sedimentation patterns: three-dimensional modeling for a tidal marsh. J. Geophys. Res. 110, F04019. doi:10.1029/2005JF000301.
Temmerman, S., Bouma, T.J., Van de Koppel, J., Van der Wal, D., De Vries, M.B., Herman, P.M.J., 2007. Vegetation causes channel erosion in a tidal landscape. Geology 35, 631–634.
Van De Wiel, M.J., Darby, S.E., 2004. Numerical modeling of bed topography and bank erosion along tree-lined rivers. In: Bennett, S.J., Simon, A. (Eds.), Riparian Vegetation and Fluvial Geomorphology. Water Science and Application 8. American Geophysical Union, Washington, D.C, pp. 267–282.
Wang, Y., Hong, W., Wu, C., He, D., Lin, S., Fan, H., 2008. Application of landscape ecology to the research on wetlands. J. Forest. Res. 19, 164–170.
Wetzel, P.R., 2002. Tree island ecosystems of the world. In: Sklar, F.H., van der Valk, A. (Eds.), Tree Islands of the Everglades. Kluwer Academic Publishers, Netherlands, pp. 19–69.
Wetzel, P., van der Valk, A.G., Newman, S., Gawlik, D.E., Troxler-Gann, T., Coronado-Molina, C., Childers, D.L., Sklar, F.H., 2005. Maintaining tree islands in the Florida Everglades: nutrient redistribution is the key. Front. Ecol. Environ. 3, 370–376.
White, B., Nepf, H.M., 2003. Scalar transport in random cylinder arrays at moderate Reynolds number. J. Fluid Mech. 487, 43–79.
White, B.L., Nepf, H.M., 2008. A vortex-based model of velocity and shear stress in a partially vegetated shallow channel. Water Resour. Res. 44. doi:10.1029/2006WR005651.
Willard, D.A., Cronin, T.M., 2007. Paleoecology and ecosystem restoration: case studies from Chesapeake Bay and the Florida Everglades. Front. Ecol. Environ. 5 (9), 491–498.
Winterwerp, J.C., van Kesteren, W.G.M., 2004. Introduction to the physics of cohesive sediment in the marine environment. Elsevier, Amsterdam.
Wootton, J.T., 2001. Local interactions predict large-scale pattern in empirically derived cellular automata. Nature 413, 841–844.
Worman, A., Kronnas, V., 2005. Effect of pond shape and vegetation heterogeneity on flow and treatment performance of constructed wetlands. J. Hydrol. 301, 123–128.
Wu, W., Wang, S.S.Y., 2004. A depth-averaged two-dimensional numerical model of flow and sediment transport in open channels with vegetation. In: Bennett, S.J., Simon, A. (Eds.), Riparian Vegetation and Fluvial Geomorphology. Water Science and Application 8. American Geophysical Union, Washington, D.C, pp. 253–266.